NASA Technical Memorandum 80086

NASA-TM-80086 19790014013

Aerodynamic Characteristics of the 140A/B Space Shuttle Orbiter at Mach 10.3

Peter T. Bernot

MAY 1979

NASA

NASA Technical Memorandum 80086

Aerodynamic Characteristics of the 140A/B Space Shuttle Orbiter at Mach 10.3

Peter T. Bernot
Langley Research Center
Hampton, Virginia

National Aeronautics
and Space Administration

Scientific and Technical
Information Office

1979

SUMMARY

Hypersonic wind-tunnel tests have been conducted to obtain the static longitudinal and lateral-directional characteristics of the 140A/B space shuttle orbiter. Data were obtained at angles of attack from 12° to 36.5° at angles of sideslip of 0° and -5°. Stability, control, and performance characteristics were determined for various deflections of elevons and body flap with the speed brake set at 55°. Tests were performed over a Reynolds number range, based on fuselage reference length, of 0.62×10^6 to 1.33×10^6, with the majority of tests made at 1.03×10^6. Effects of aileron deflection on roll control and longitudinal stability were also determined.

With the center of gravity located at 65 percent of fuselage length, the orbiter is neutrally stable at a 20° angle of attack for elevons and body flap set at 0° deflection. For a typical entry attitude of 30°, stable trim conditions can be achieved with a resulting lift-drag ratio of 1.40. Deflecting the body flap can provide additional trim capability. Increase of the Reynolds number causes higher values of lift-drag ratio, but only for angles of attack up to 24°.

The orbiter is directionally unstable over the angle-of-attack range with positive dihedral effect. Increasing the speed-brake angle from 55° to 85° slightly improves dihedral effectiveness.

Aileron deflection results in adverse yaw to roll control over the test angle-of-attack range. In addition, significant negative increments of pitching-moment coefficient occur which affect orbiter trim and stability.

INTRODUCTION

The space shuttle transportation system described in references 1 and 2 is now well underway. The approach and landing flight tests were completed successfully in 1977. A portion of the low-speed flight characteristics of the full-scale orbiter vehicle can now be evaluated with a high degree of confidence. However, flight data at the higher speed regimes will only be obtained from the orbital flight test program with the first launch now scheduled for the end of 1979. Consequently, predictions of the aerodynamic characteristics of the orbiter at these higher speeds must rely on wind-tunnel test results and theoretical analysis.

This report presents the longitudinal and lateral-directional characteristics of a 0.010-scale version of the 140A/B orbiter obtained experimentally at a free-stream Mach number of 10.3. Static stability, control, and performance data were obtained over an angle-of-attack range from 12° to 36.5° at various elevon and body-flap deflections with the speed brake set at 55°. The majority of tests were conducted at a Reynolds number of 1.03×10^6 based on fuselage reference length; additional tests were made at Reynolds numbers of 0.63×10^6

and 1.33×10^6 for selected control deflections. Lateral-directional data were generated by testing the model at a sideslip angle of -5° and included effects of control deflections and increasing the speed-brake deflection angle from 55° to 85°.

In addition, roll-control effectiveness was determined for aileron angles of up to 15° at an elevon deflection of 0° and included effects on the longitudinal stability characteristics.

This investigation, designated "Rockwell International test 0A90," was conducted in the Langley continuous-flow hypersonic tunnel and used a six-component, water-cooled balance to measure forces and moments. The complete test results are tabulated in reference 3.

SYMBOLS

The longitudinal characteristics are based on both the body- and stability-axis systems. The lateral-directional characteristics are based on the body-axis system only. Measurements and calculations were made in the U.S. Customary Units. Values are presented herein in the International System of Units (SI) with the equivalent values in the U.S. Customary Units given parenthetically.

b model reference wing span, m (in.)

C' Chapman-Rubesin constant based on reference temperature, $\mu'T/\mu T'$

C_A axial-force coefficient, $\frac{\text{Axial force}}{qS}$

C_D drag coefficient, $\frac{\text{Drag force}}{qS}$

C_L lift coefficient, $\frac{\text{Lift force}}{qS}$

C_l rolling-moment coefficient, $\frac{\text{Rolling moment}}{qSb}$

C_{l_β} effective dihedral parameter, $\Delta C_l/\Delta\beta$, per deg

$C_{l_{\delta_a}}$ rate of change of rolling-moment coefficient with aileron deflection angle, $\Delta C_l/\Delta\delta_a$, per deg

C_m pitching-moment coefficient, $\frac{\text{Pitching moment}}{qS\bar{c}}$

C_N normal-force coefficient, $\dfrac{\text{Normal force}}{qS}$

C_n yawing-moment coefficient, $\dfrac{\text{Yawing moment}}{qSb}$

C_{n_β} directional-stability parameter, $\Delta C_n/\Delta\beta$, per deg

$\left(C_{n_\beta}\right)_{dyn}$ dynamic directional-stability parameter, $C_{n_\beta} \cos \alpha - C_{l_\beta} \dfrac{I_Z}{I_X} \sin \alpha$, per deg

$C_{n_{\delta_a}}$ rate of change of yawing-moment coefficient with aileron deflection angle, $\Delta C_n/\Delta\delta_a$, per deg

C_Y side-force coefficient, $\dfrac{\text{Side force}}{qS}$

C_{Y_β} rate of change of side-force coefficient with sideslip angle, $\Delta C_Y/\Delta\beta$, per deg

$C_{Y_{\delta_a}}$ rate of change of side-force coefficient with aileron deflection angle, $\Delta C_Y/\Delta\delta_a$, per deg

$\bar{c}$ wing mean aerodynamic chord, m (in.)

I_Z/I_X ratio of moments of inertia about yaw and roll axes, respectively

L/D lift-drag ratio

l fuselage reference length, m (in.)

M free-stream Mach number

q free-stream dynamic pressure

p pressure, Pa (psia)

R_l Reynolds number based on fuselage length and free-stream conditions

S wing total planform reference area, m^2 (ft^2)

T temperature, K (^{o}F)

$\bar{V}'_\infty$ viscous interaction parameter, $M\left(\dfrac{C'}{R_l}\right)^{1/2}$

α	angle of attack, deg
β	angle of sideslip, deg
γ	ratio of specific heats
δ_a	aileron deflection angle, $\frac{\delta_{e,L} - \delta_{e,R}}{2}$, deg
δ_e	elevon deflection angle, $\frac{\delta_{e,L} + \delta_{e,R}}{2}$, positive for trailing edge down, deg
δ_{BF}	body-flap deflection angle, positive for trailing edge down, deg
δ_{SB}	speed-brake deflection angle, deg
μ	dynamic viscosity

Subscripts:

L	left
max	maximum
R	right
w	model wall
t	tunnel stagnation conditions
∞	free-stream conditions
$.65l$	moment center 65 percent of fuselage length

Abbreviations:

FRL	fuselage reference line
IML	inner mold line
OML	outer mold line
OMS	orbital maneuver system

Model component designations:

B_{26}	fuselage
C_9	canopy

E_{37} elevons with V-slots

F_{10} updated body flap

M_7 OMS pods

N_{28} OMS engine nozzles

R_5 rudder

V_8 vertical tail

W_{116} wing

A prime used after a symbol refers to reference conditions.

MODEL DESCRIPTION

The test model was a 0.010-scale version of the 140A/B space shuttle orbiter which was fabricated from aluminum alloy by Rockwell International and designated "model 72-0." As shown in the sketch of figure 1(a), the model had full-span split elevons, a vertical tail, and a body flap. The OMS nozzles were incorporated on the model; however, the three main rocket nozzles at the base of the configuration were omitted to allow installation of the balance and sting. Elevon deflection angles were set by using small prebent brackets; the body flap and speed brakes used separate interchangeable components for each deflection angle. Definitions of deflection angle for these controls are presented in figure 1(b). This model was slightly modified in comparison to previous versions of the 140A/B orbiter. These modifications consisted of using an updated body flap and having a V-shaped slot between the split elevons. The various model components as defined by Rockwell International are shown in figure 1(c) and are listed as follows:

B_{26} fuselage

C_9 canopy

W_{116} wing

E_{37} elevons with V-slots

M_7 OMS pods

N_{28} OMS engine nozzles

F_{10} updated body flap

V_8 vertical tail

R_5 rudder

The full-scale geometric characteristics of these components are presented in table I.

APPARATUS

This investigation was conducted in the Mach 10 nozzle of the Langley continuous-flow hypersonic tunnel which is designed to operate at stagnation pressures of 15 to 150 atm (1 atm = 101 kPa) at temperatures up to 1089 K (1500° F). The nozzle has a 0.79-m- (31.0-in-) square test section and is equipped with a movable second minimum section. To prevent liquefaction, air is preheated electrically by passing it through a multitube heater. For continuous operation, the air is circulated through this closed-circuit facility by a series of five compressors. Operation in the blowdown mode is also possible by drawing the exiting flow into a vacuum sphere.

This facility utilizes a hydraulically actuated injection/retraction mechanism contained within a sealed chamber which is mounted adjacent to the test section wall (fig. 2(a)). The chamber can be rotated about a vertical axis which permits easy access to the test model without disruption of tunnel flow (fig. 2(b)). Two L-shaped pressurized air rakes, mounted in actuators, are discernible inside the chamber and are regularly used for rapid model cooling after each test run. Model forces and moments are measured by water-cooled balances which are equipped with thermocouple wires for monitoring balance temperatures. A specially designed computer system is normally used for recording force data over the angle-of-attack range using a pitch-pause mode. The selected angles of attack and sideslip, duration of pause time, and data recording are inputted to this system, resulting in a completely automatic operation. Overall details of this facility are presented in reference 4.

TESTS

Force and moment data were obtained by a six-component strain-gage balance which was mounted in a 20° prebent sting. A photograph of the model-sting assembly is presented in figure 3. The orbiter model was tested over an angle-of-attack range of 12° to 36.5° at sideslip angles of 0° and -5°. The lateral-directional coefficient derivatives were calculated by assuming linearity between the basic data measured at these sideslip angles. Data were obtained for several elevon deflection angles ranging from -40° to 15° while body-flap deflection angles were limited to -11.7°, 0°, and 16.3°. The majority of tests were made at a Reynolds number of 1.03×10^6 based on fuselage reference length. Additional tests were also performed at Reynolds numbers of 0.63×10^6 and 1.33×10^6 at selected control deflection angles. A summary of tunnel test conditions is presented in the following table:

p_t		T_t		M	R_l	$\bar{v}'_\infty$
MPa	psia	K	°F			
3.24	470	1023	1381	10.31	0.64×10^6	0.0117
5.06	734	1012	1362	10.33	1.03	.0092
6.62	960	1019	1374	10.37	1.33	.0082

Values of the viscous interaction parameter $\bar{v}'_\infty$ were calculated from the equations presented in the appendix of reference 5. For completeness, they are repeated as follows:

$$\bar{v}'_\infty = M\left(\frac{C'}{R_l}\right)^{1/2}$$

where

$$C' = \left(\frac{T'}{T_\infty}\right)^{1/2}\left[\frac{T_\infty + 122.1 \times 10^{-(5/T_\infty)}}{T' + 122.1 \times 10^{-(5/T')}}\right]$$

and

$$\frac{T'}{T_\infty} = 0.468 + 0.532 \frac{T_w}{T_\infty} + 0.195 \frac{(\gamma - 1)}{2} M^2$$

where $T_w = 367$ K.

Real-gas correction factors were calculated from reference 6 to determine tunnel-flow properties. In addition, sting-deflection constants were obtained prior to the tests and were used in calculating true angles of attack and sideslip.

Estimated inaccuracies in the measured balance data are based on ±1/2 percent of balance design load. For the tests at $R_l = 1.03 \times 10^6$, these inaccuracies expressed in coefficient form are as follows:

$C_N = \pm 0.0090$ $C_l = \pm 0.0002$

$C_A = \pm 0.0020$ $C_n = \pm 0.0003$

$C_m = \pm 0.0018$ $C_Y = \pm 0.0030$

For tests at $R_l = 0.64 \times 10^6$, these values should be multiplied by 1.574; for the tests at the higher Reynolds number, the multiplier value is 0.784. Accuracy of the angles of attack and sideslip is ±0.1°, and accuracy for free-stream Mach number is ±0.02. In this investigation, model base pressures were not measured.

DISCUSSION OF RESULTS

Longitudinal Aerodynamic Characteristics

The longitudinal characteristics for combined deflections of the elevons and body flap are presented in figure 4. For the center-of-gravity location at 65 percent of fuselage length, the orbiter is neutrally stable at an angle of attack of approximately 20° with both controls set at 0°. (See fig. 4(b).) Maximum values of L/D range from 1.90 to 1.78. These values occur at angles of attack of 16° to 20°, respectively. However, entry trajectory studies based on heating constraints have indicated that a 30° angle of attack is a more realistic value for a flight speed of Mach 10 and a resulting flight Reynolds number of 6×10^6. Stable trim can be obtained at this attitude by deflecting the elevons a few degrees negatively (trailing edge up) which results in a L/D value of about 1.40. In figure 5, the effects of body-flap deflections at an elevon setting of 0° are presented. For a positive deflection of 16.3°, the body flap produced sizable increments in C_m, especially at angles of attack greater than 20°, whereas the negatively deflected body flap yielded much smaller increments (fig. 5(b)). In general, the body flap can provide some additional control power without any reduction in L/D.

A summary plot for all elevon and body-flap deflection angles is presented in figure 6 where α and C_m are plotted against C_N. This figure, as presented, can be used to determine trim and stability at center-of-gravity locations other than the 65-percent station. An example is shown in this figure for a center-of-gravity location at 66 percent. Rotating the C_m axis (indicated by the dashed line) shows that the orbiter can have a stable trim point at $\alpha = 37°$ with zero deflections on both controls. Some data extrapolation is required for this example.

The effects of sealing the V-slots between the split elevons are shown in figure 7 for positive deflections of both controls. As expected, these effects are quite small.

The effects of Reynolds numbers are presented in figure 8 for the control deflections set at full up, zero, and full down. As shown in figure 8(b), the major effect of increasing Reynolds number was to decrease axial force (drag) by reducing skin friction. This effect resulted in increases of L/D at angles of attack up to about 24°. The highest value of $(L/D)_{max}$ was 1.90 at a 17.3° angle of attack for zero control deflections. Reducing the Reynolds number to 0.63×10^6 caused a reduction of $(L/D)_{max}$ to 1.81 at an angle of attack of 17.7°. For a flight Reynolds number of 6×10^6, higher values of $(L/D)_{max}$ could be expected. Other aerodynamic characteristics were only slightly affected by variation of Reynolds number in this investigation.

Lateral-Directional Aerodynamic Characteristics

The variations of C_l, C_n, and C_Y with angle of sideslip are presented in figure 9 for angles of attack of 20° and 30°. The purpose of this figure is to determine the extent of linearity of these coefficients. The results indicate that linearity does exist for angles of sideslip up to at least -5°, thus validating the technique used for the lateral-directional results presented in figure 10.

The effects of elevon, body-flap, and speed-brake deflection on the sideslip characteristics are presented in figure 10 for Reynolds numbers of 1.03×10^6 and 1.33×10^6. In all cases, positive effective dihedral $-C_{l_\beta}$ is indicated over the test angle-of-attack range; however, the orbiter is directionally unstable. Favorable (positive) values of the dynamic directional-stability parameter are obtained which increase with angle of attack. The effects of elevon and body-flap deflection are best illustrated by the data at the higher Reynolds number presented in figure 10(b). Positive elevon control deflections cause a small improvement in effective dihedral $-C_{l_\beta}$ while negative deflections clearly result in a decrease in this parameter. In general, the effects on C_{n_β} are essentially negligible. Increasing the speed-brake angle from 55° to 85° yields a small increase in dihedral effectiveness with little change in C_{n_β}. These effects are expected since the vertical tail is shielded from the flow for the test angle-of-attack range of this investigation.

Aileron Effects on Aerodynamic Characteristics

The effects of varying aileron deflection angle on rolling moment, yawing moment, and side-force derivatives are presented in figure 11 for a constant elevon deflection angle of 0°. The aileron deflection angles were 5°, 10°, and 15° and are positive as defined in the section "Symbols" in this paper. Roll-control effectiveness $C_{l_{\delta_a}}$ increased with angle of attack and was only slightly affected by aileron deflection angle. Negative values of $C_{n_{\delta_a}}$ are obtained, resulting in adverse yaw due to roll control over the angle-of-attack range. Consequently, the values for the ratio of $C_{n_{\delta_a}}$ to $C_{l_{\delta_a}}$ are negative and remain essentially constant with increasing angle of attack.

In figure 12, the effects of aileron deflection angle on the longitudinal characteristics are presented. Significant negative increments in C_m are obtained as aileron angle was increased which, for this case, results in an unfavorable effect on orbiter trim as shown in figure 12(b). These negative increments are caused by the greater effectiveness of the elevon going down into the airstream. Some reduction in L/D is seen to occur; however, these performance losses are small.

SUMMARY OF RESULTS

Longitudinal and lateral-directional characteristics have been determined for the 140A/B space shuttle orbiter at a free-stream Mach number of 10.3 over an angle-of-attack range of 12° to 36.5°. Tests were conducted over a range of Reynolds numbers, based on fuselage reference length, of 0.63×10^6 to 1.33×10^6. Effects of aileron deflection were also obtained. The results of this investigation are presented about a center-of-gravity location at 65 percent of fuselage length and are summarized as follows:

1. The orbiter is neutrally stable at an angle of attack of approximately 20° with elevons and body flap deflected 0°.

2. At a typical entry attitude of 30°, stable trim can be achieved with a lift-drag ratio of about 1.40.

3. Deflection of the body flap can provide some additional trim capability.

4. Increasing the Reynolds number causes higher values of lift-drag ratio, but only for angles of attack up to about 24°.

5. The orbiter is directionally unstable over the angle-of-attack range with positive dihedral effect. Increasing the speed-brake deflection from 55° to 85° slightly improves effective dihedral with little change in directional stability.

6. Aileron deflection results in adverse yaw to roll control for all angles of attack. In addition, sizable negative increments of pitching-moment coefficient occur, thus affecting the trim and stability of the orbiter.

Langley Research Center
National Aeronautics and Space Administration
Hampton, VA 23665
April 6, 1979

REFERENCES

1. Malkin, M. S.: Space Shuttle/The New Baseline. Astronaut. & Aeronaut., vol. 12, no. 1, Jan. 1974, pp. 62-78.

2. Space Shuttle. NASA SP-407, 1976.

3. Hawthorne, P. J.: Results of Investigations on a 0.010-Scale 140A/B Configuration Space Shuttle Vehicle Orbiter Model 72-0 in the NASA Langley Research Center Continuous Flow Hypersonic Tunnel (OA90). NASA CR-141,805, 1975.

4. Schaefer, William T., Jr.: Characteristics of Major Active Wind Tunnels at the Langley Research Center. NASA TM X-1130, 1965.

5. Bertram, Mitchel H.: Hypersonic Laminar Viscous Interaction Effects on the Aerodynamics of Two-Dimensional Wedge and Triangular Planform Wings. NASA TN D-3523, 1966.

6. Erickson, Wayne D.; and Creekmore, Helen S.: A Study of Equilibrium Real-Gas Effects in Hypersonic Air Nozzles, Including Charts of Thermodynamic Properties for Equilibrium Air. NASA TN D-231, 1960.

TABLE I.- FULL-SCALE GEOMETRIC CHARACTERISTICS OF THE

140A/B SPACE SHUTTLE ORBITER

Body, B_{26}:	
Length (measured from OML), m (in.)	32.85 (1293.3)
Length (measured from IML), m (in.)[a]	32.77 (1290.3)
Maximum width, m (in.)	6.65 (262.0)
Maximum depth, m (in.)	6.35 (240.0)
Fineness ratio	4.93
Canopy, C_9:	
Length, m (in.)	3.64 (143.3)
Maximum width, m (in.)	3.87 (152.4)
Maximum depth, m (in.)	0.63 (25.0)
Wing, W_{116}:	
Planform area (theoretical), m^2 (ft^2)[a]	249.91 (2690.0)
Span, m (in.)[a]	23.79 (936.7)
Aspect ratio	2.26
Dihedral angle, deg	3.50
Incidence angle, deg	0.50
Sweepback angle (leading edge), deg	45.00
Sweepback angle (trailing edge), deg	-10.05
Aerodynamic twist, deg	3.00
Mean aerodynamic chord, m (in.)[a]	12.06 (474.8)
Root chord (theoretical), m (in.)	17.51 (689.2)
Tip chord (theoretical), m (in.)	3.50 (137.8)
Airfoil section at root	Modified NACA 0011.3-64
Airfoil section at tip	Modified NACA 0012-64
Fillet total planform area, m^2 (ft^2)	21.99 (236.7)
Fillet sweepback angle, deg	81
Elevon, E_{37} (for one side):	
Planform area, m^2 (ft^2)	19.51 (210.0)
Span (equivalent), m (in.)	8.87 (349.2)
Inboard chord (equivalent), m (in.)	2.99 (118.0)
Outboard chord (equivalent), m (in.)	1.40 (55.2)
Sweepback angle at leading edge, deg	0.00
Sweepback angle at trailing edge, deg	-10.05
Body flap, F_{10}:	
Area, m^2 (ft^2)	12.42 (133.7)
Span (equivalent), m (in.)	6.42 (255.4)
Inboard chord (equivalent), m (in.)	2.06 (81)
Outboard chord (equivalent), m (in.)	2.06 (81)
Sweepback angle at hinge line, deg	0.00
Sweepback angle at trailing edge, deg	0.00

[a]Reference values.

TABLE I.- Concluded

Vertical tail, V_8:	
Planform area (theoretical), m^2 (ft^2)	38.39 (413.2)
Span (theoretical), m (in.)	8.02 (315.7)
Aspect ratio	1.67
Sweepback angle at leading edge, deg	45.00
Sweepback angle at trailing edge, deg	25.95
Root chord (theoretical), m (in.)	6.82 (268.5)
Tip chord (theoretical), m (in.)	2.76 (108.5)
Airfoil section -	
Leading wedge angle, deg	10.00
Trailing wedge angle, deg	14.92
Rudder, R_5:	
Area, m^2 (ft^2)	9.88 (106.4)
Span (equivalent), m (in.)	5.11 (201.0)
Inboard chord, m (in.)	2.33 (91.6)
Outboard chord, m (in.)	1.29 (50.8)
Sweepback angle at hinge line, deg	34.83
Sweepback angle at trailing edge, deg	26.25
OMS pod, M_7:	
Length, m (in.)	8.31 (327.0)
Maximum width, m (in.)	2.40 (94.5)
Maximum depth, m (in.)	2.77 (109.0)
OMS nozzles, N_{28}:	
Left/right nozzle	
Null pitch angle, deg	15.82
Null yaw angle, deg	12.28
Gimbal pitch range, deg	±8.0
Gimbal yaw range -	
Outboard, deg	13.28
Inboard, deg	2.28

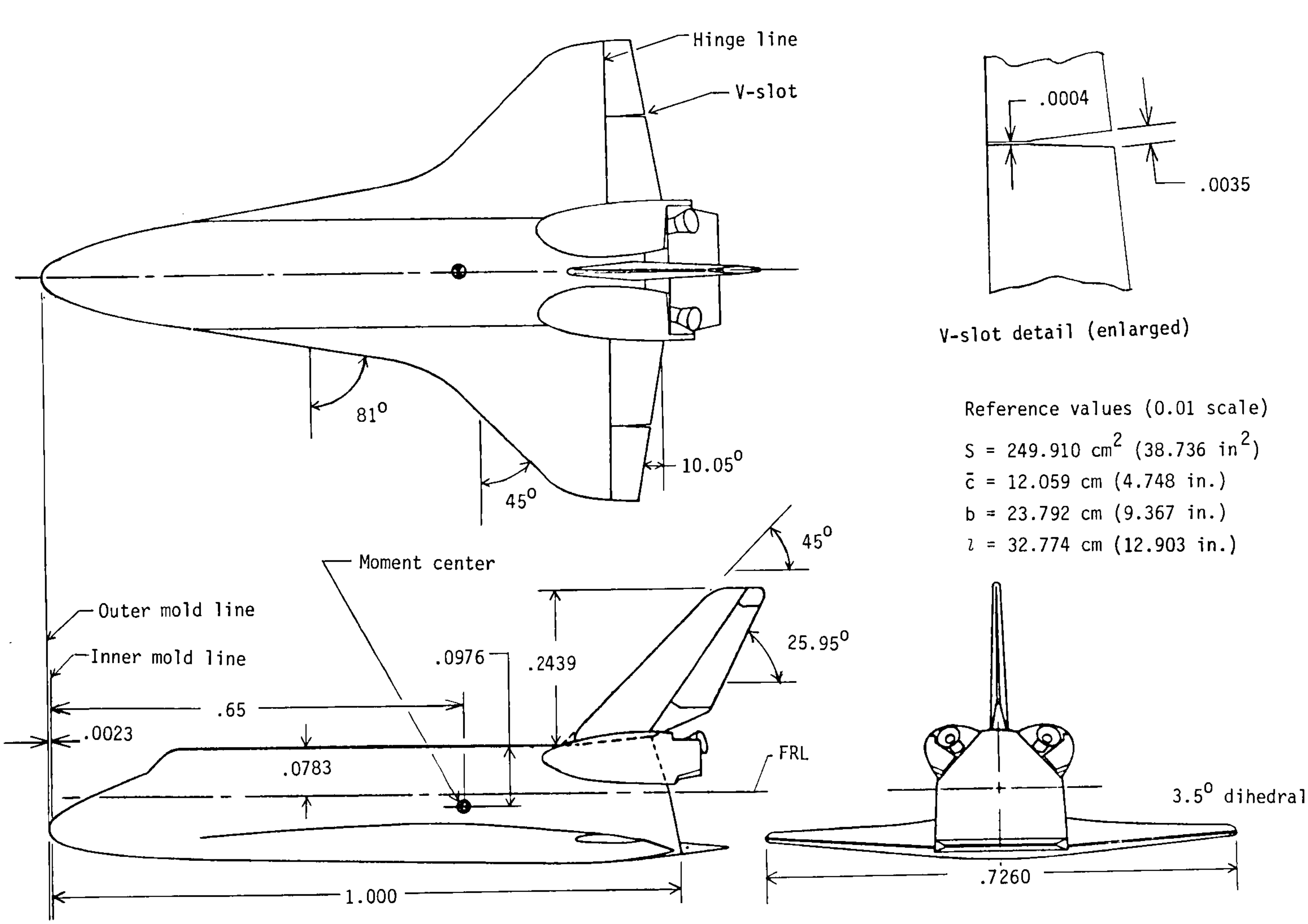

(a) Model details.

Figure 1.- Sketch of test model of 140A/B space shuttle orbiter (model 72-0). Dimensions are normalized by reference length l.

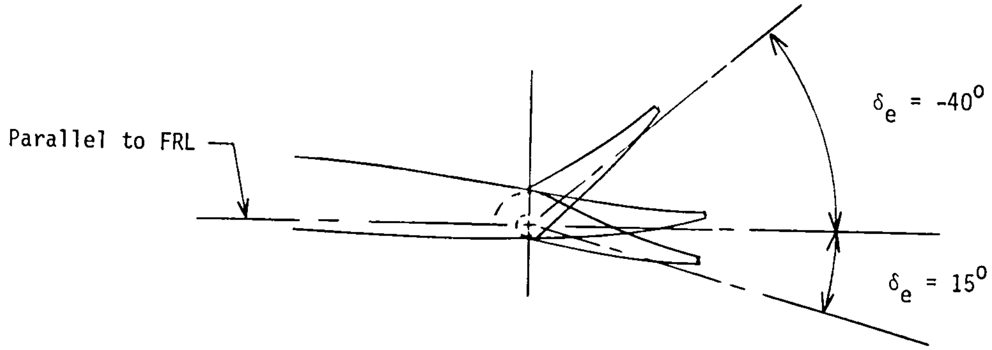

Elevon deflections

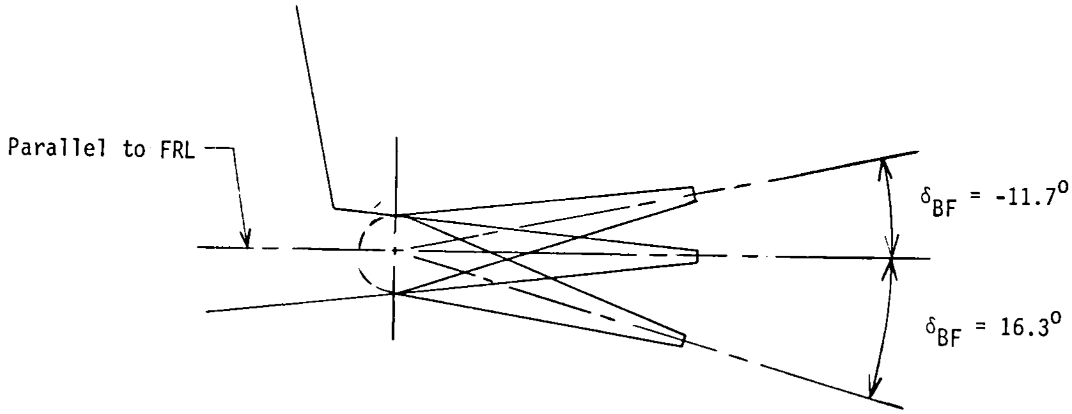

Body-flap deflections

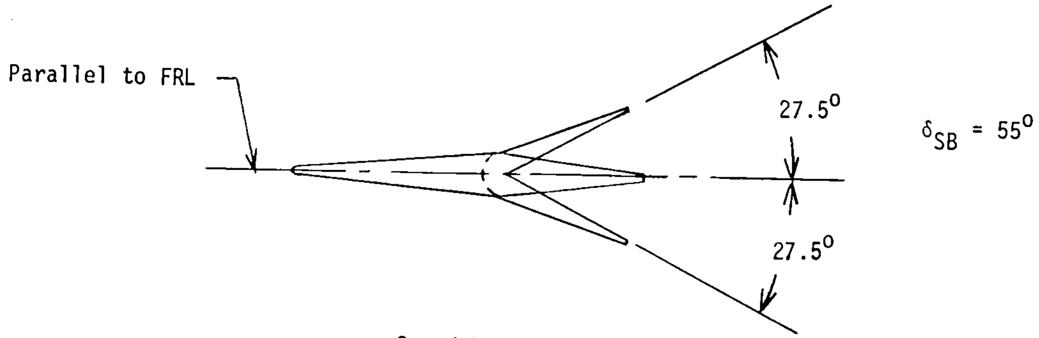

Speed brake deflection

(b) Definition of control deflection angles.

Figure 1.- Continued.

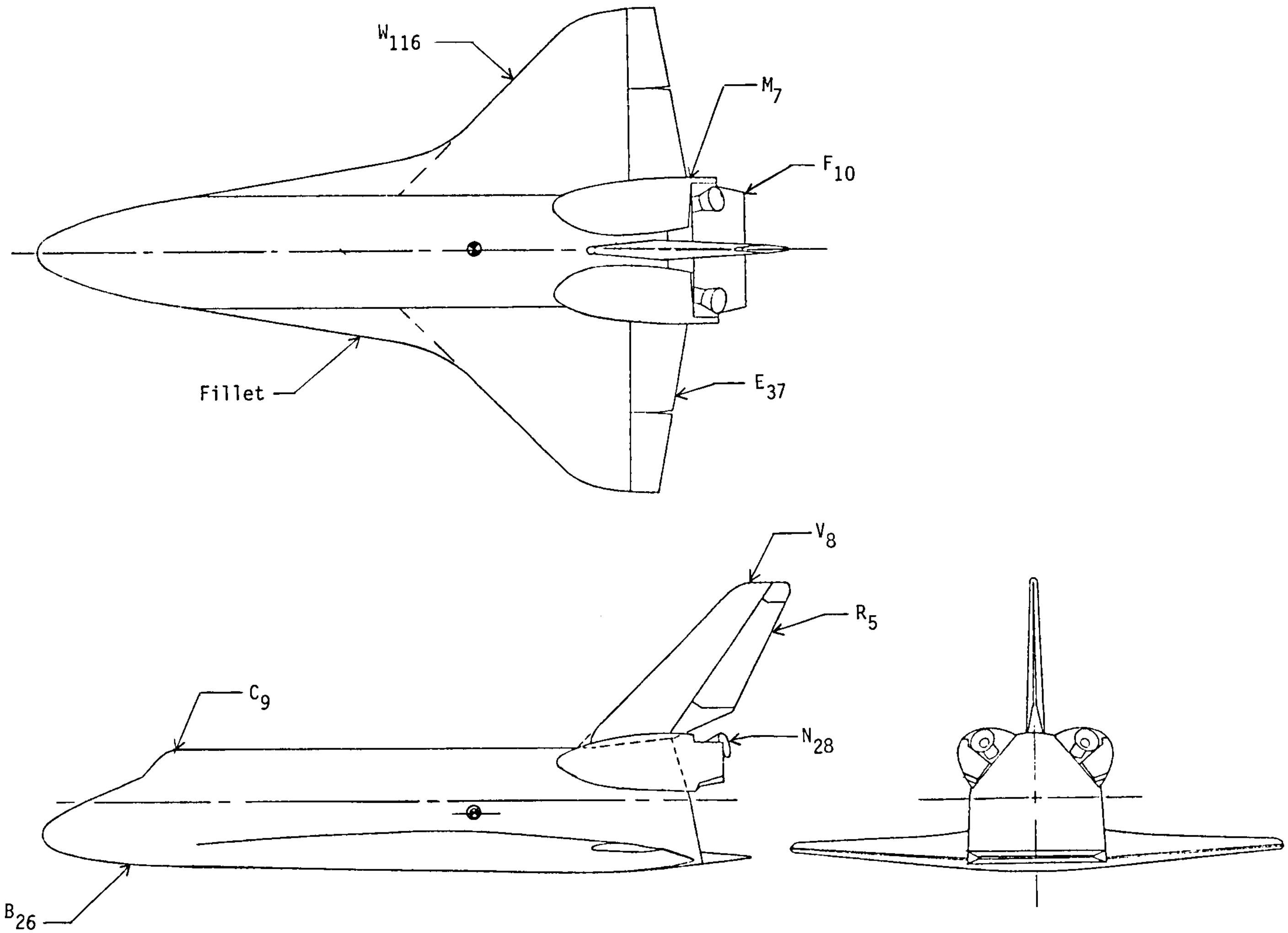

(c) Designations of model components.

Figure 1.- Concluded.

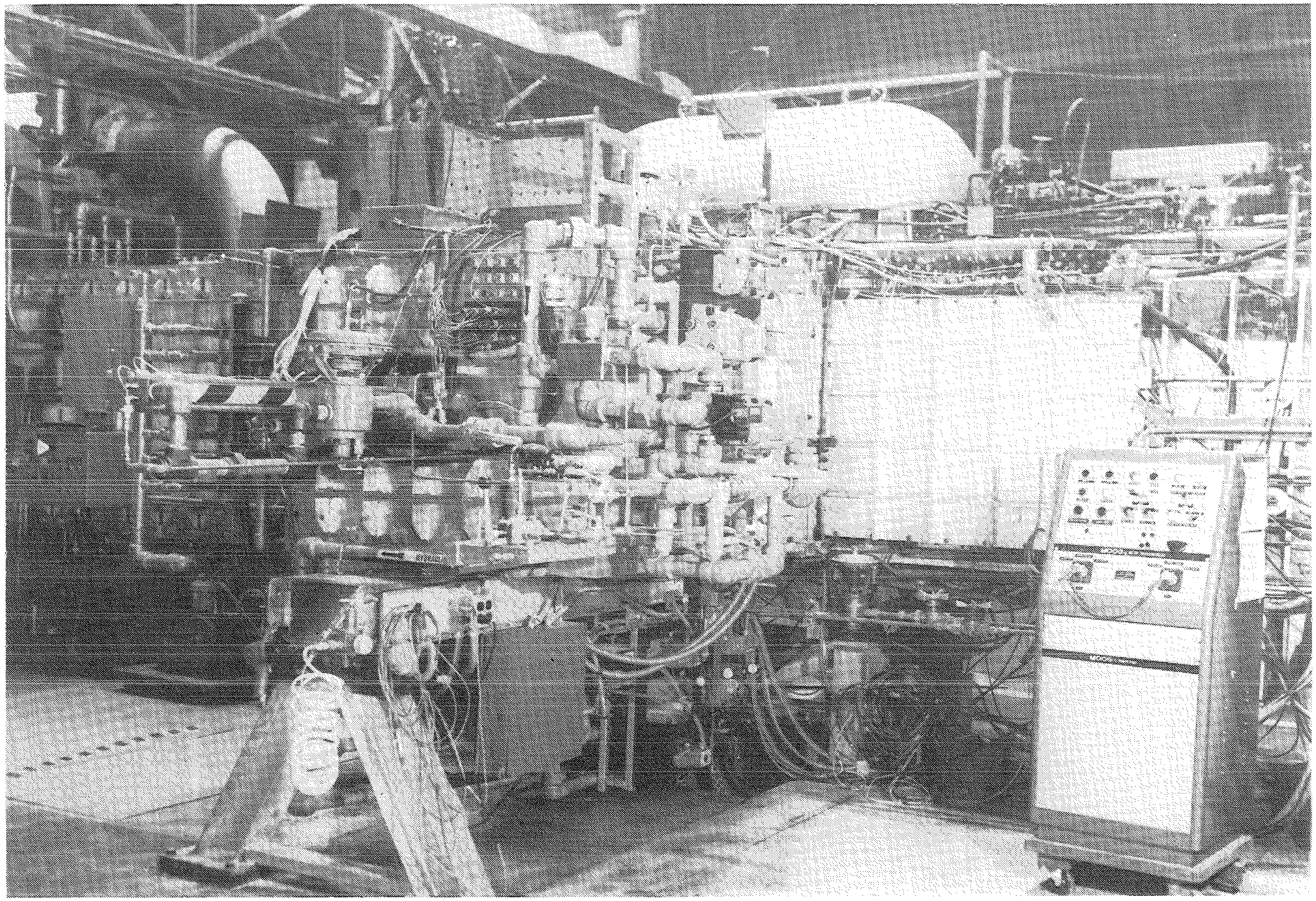

L-74-845

(a) In closed position.

Figure 2.- Photographs of rotatable sealed chamber located at tunnel test section.

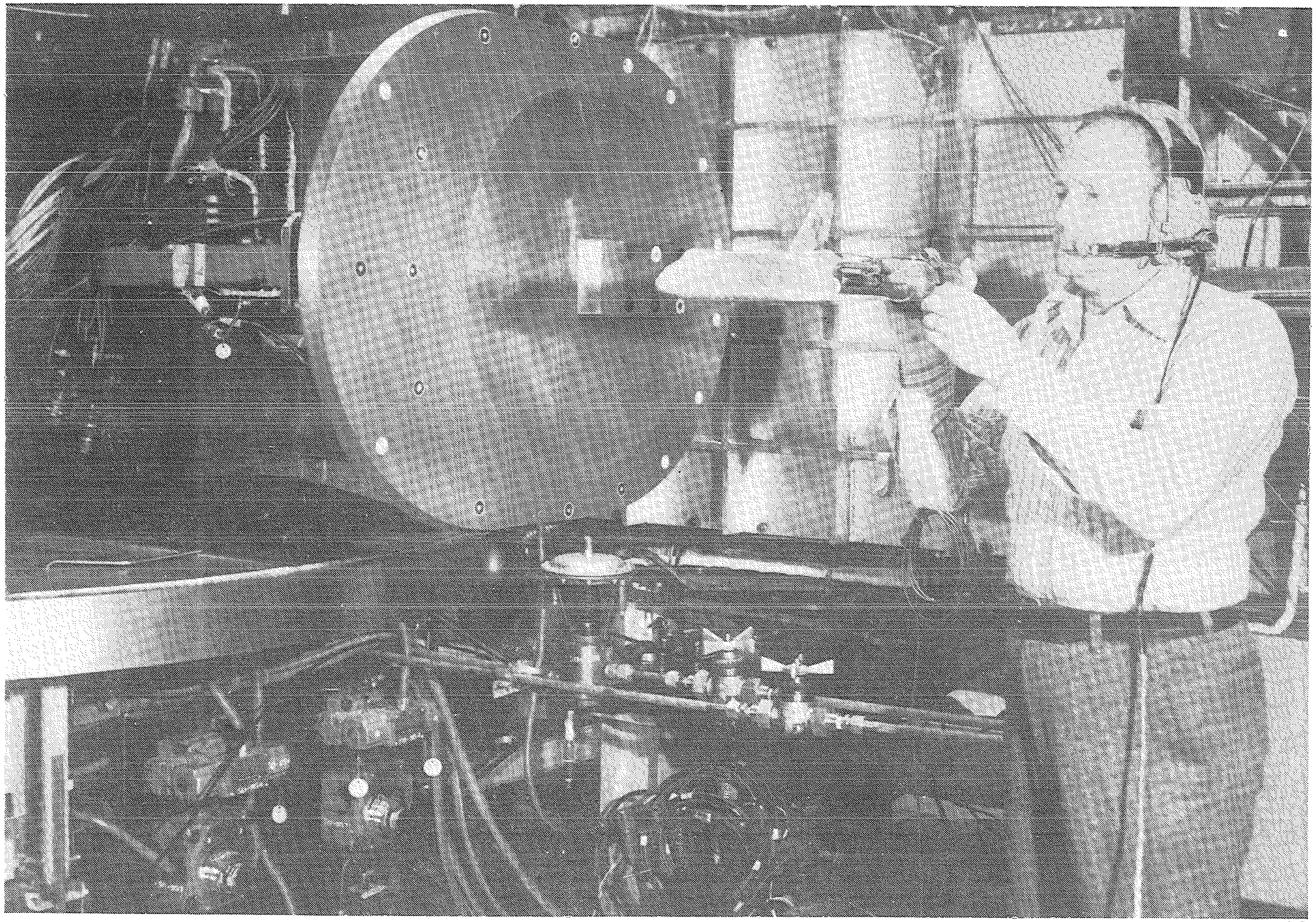

L-74-846

(b) In open position.

Figure 2.- Concluded.

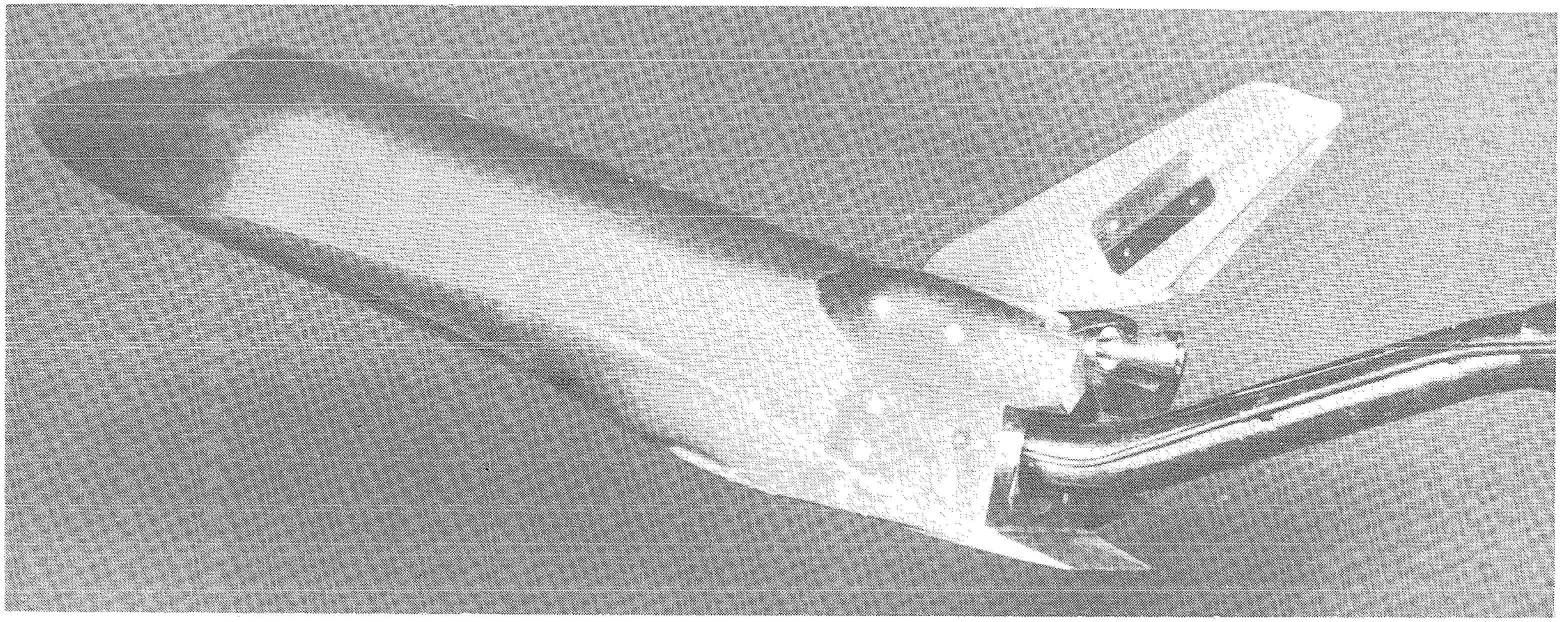

L-74-991

Figure 3.- Model-sting setup in Langley continuous-flow hypersonic tunnel.

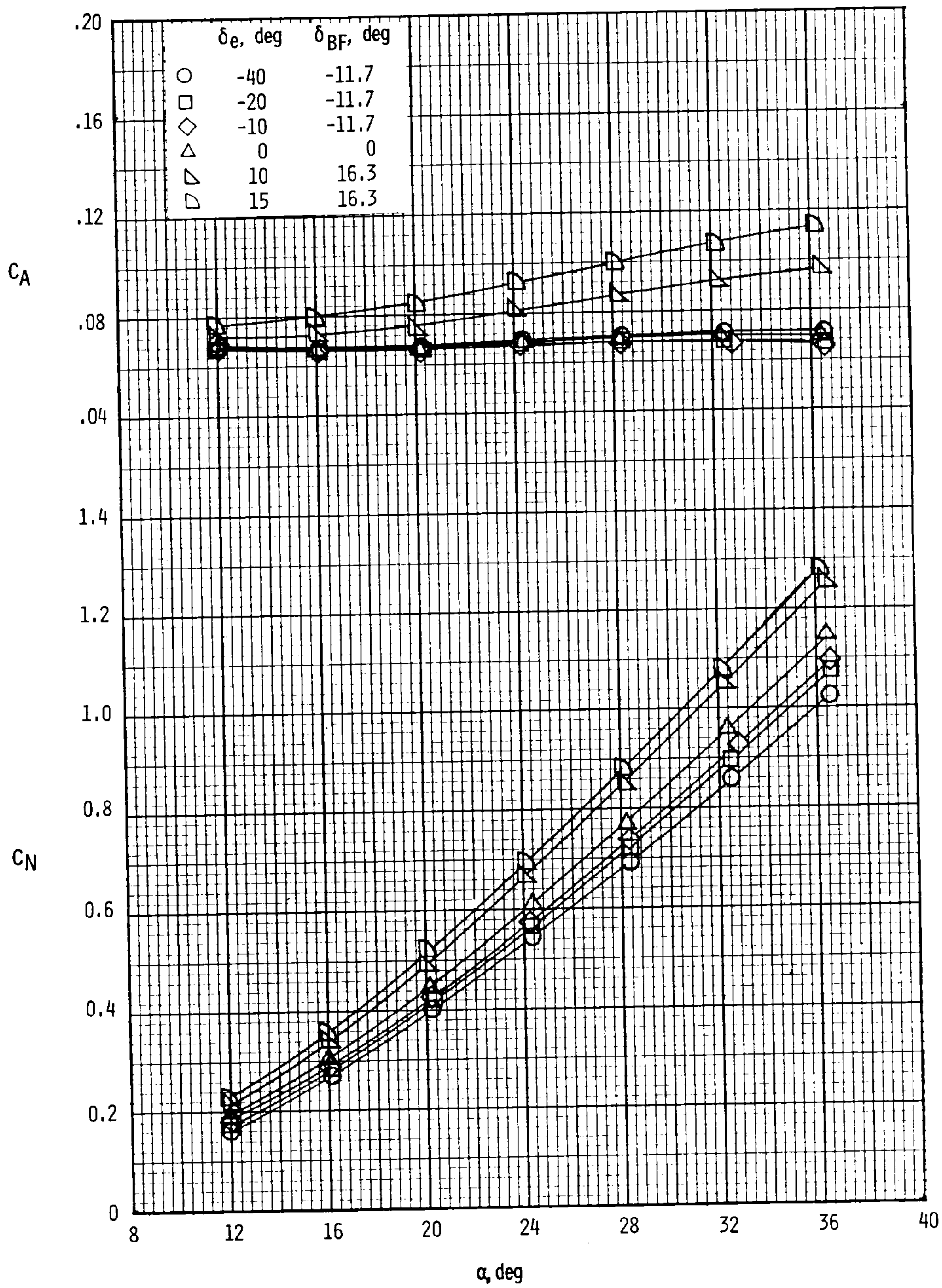

(a) C_A and C_N plotted against α.

Figure 4.- Effects of elevon and body-flap deflections on longitudinal characteristics. $\delta_{SB} = 55^{\circ}$; $R_l = 1.03 \times 10^6$.

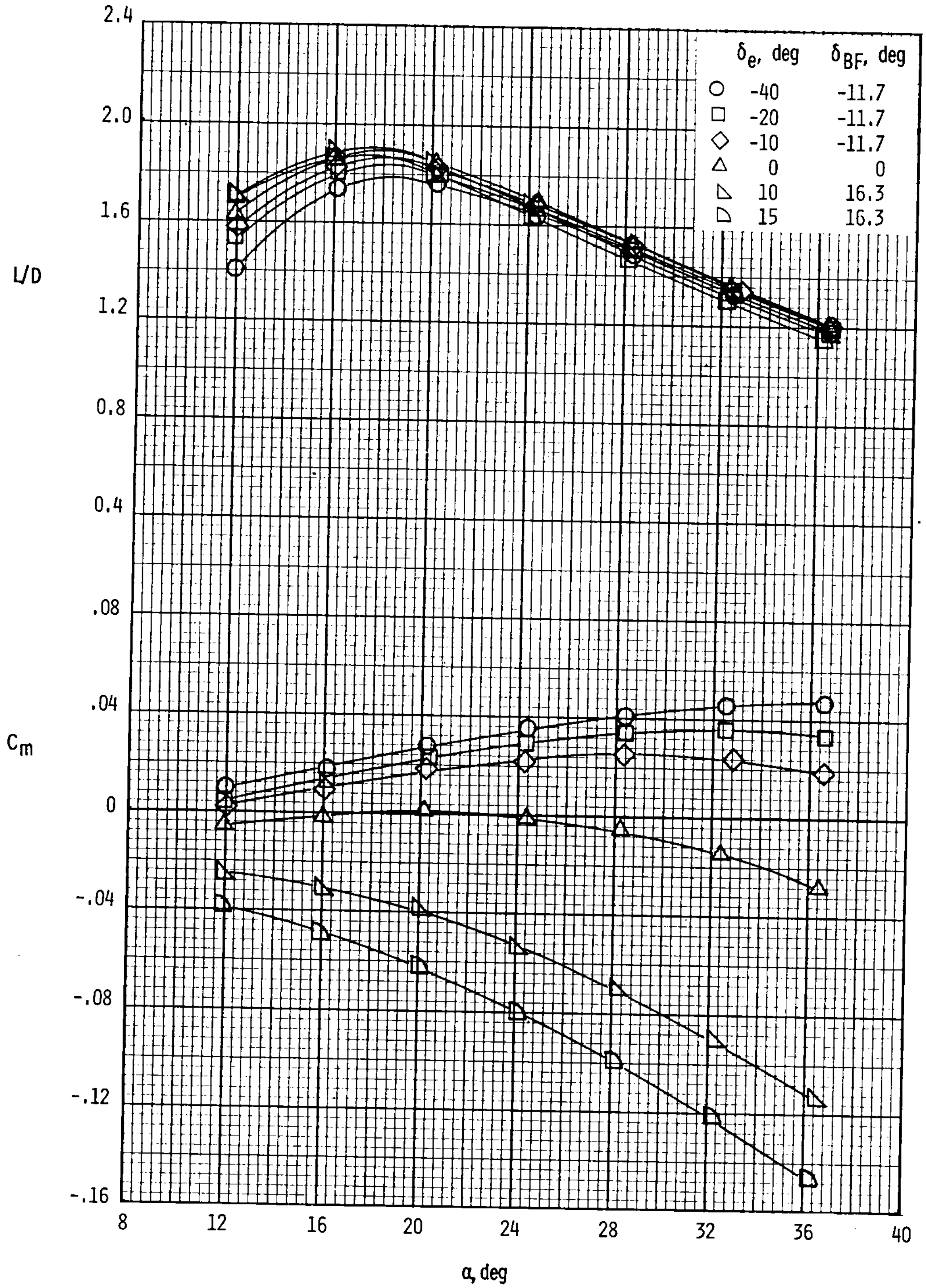

(b) L/D and C_m plotted against α.

Figure 4.- Continued.

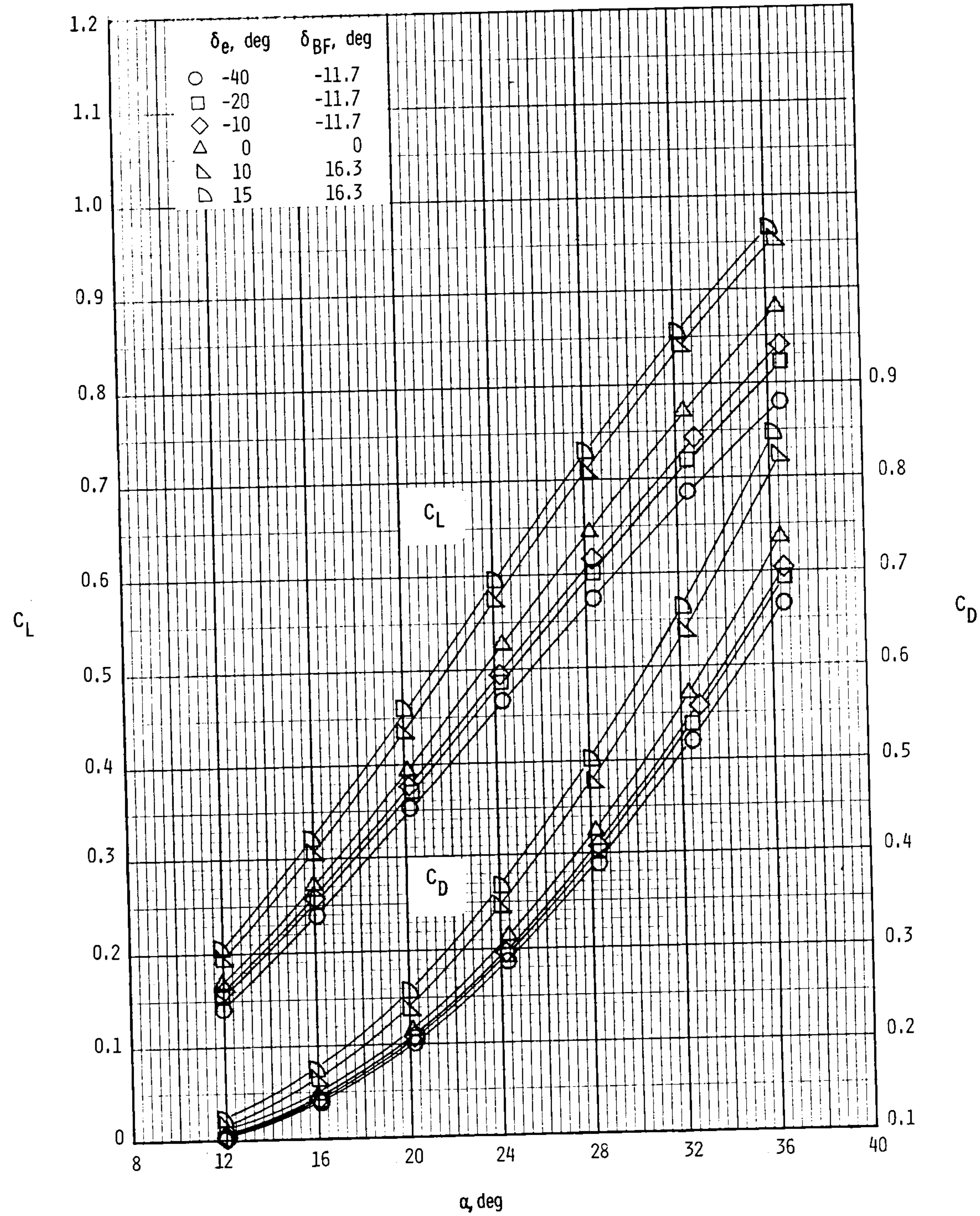

(c) C_L and C_D plotted against α.

Figure 4.- Continued.

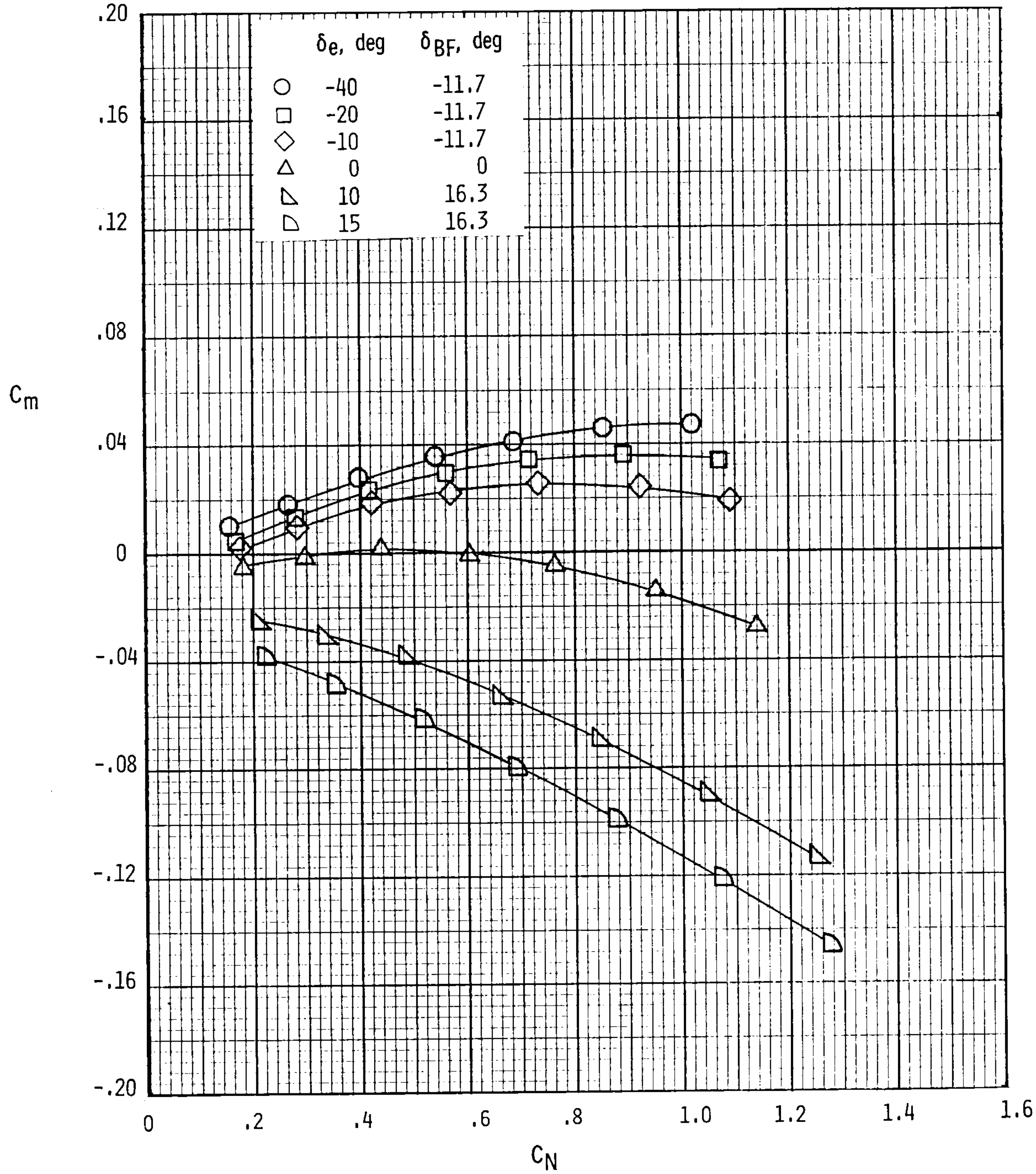

(d) C_m plotted against C_N.

Figure 4.- Concluded.

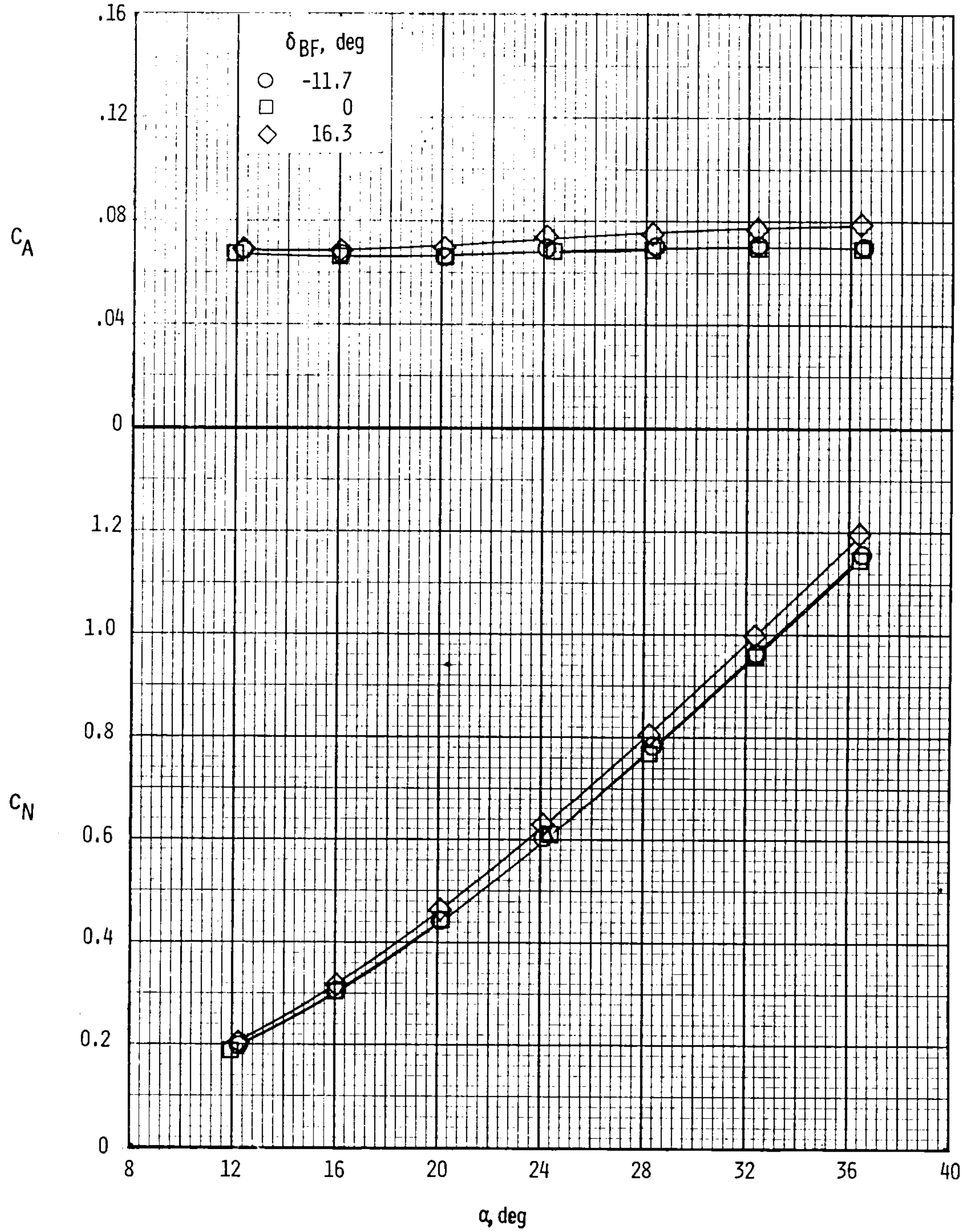

(a) C_A and C_N plotted against α.

Figure 5.- Effects of body-flap deflections on longitudinal characteristics. $\delta_e = 0^\circ$, $\delta_{SB} = 55^\circ$, and $R_l = 1.03 \times 10^6$.

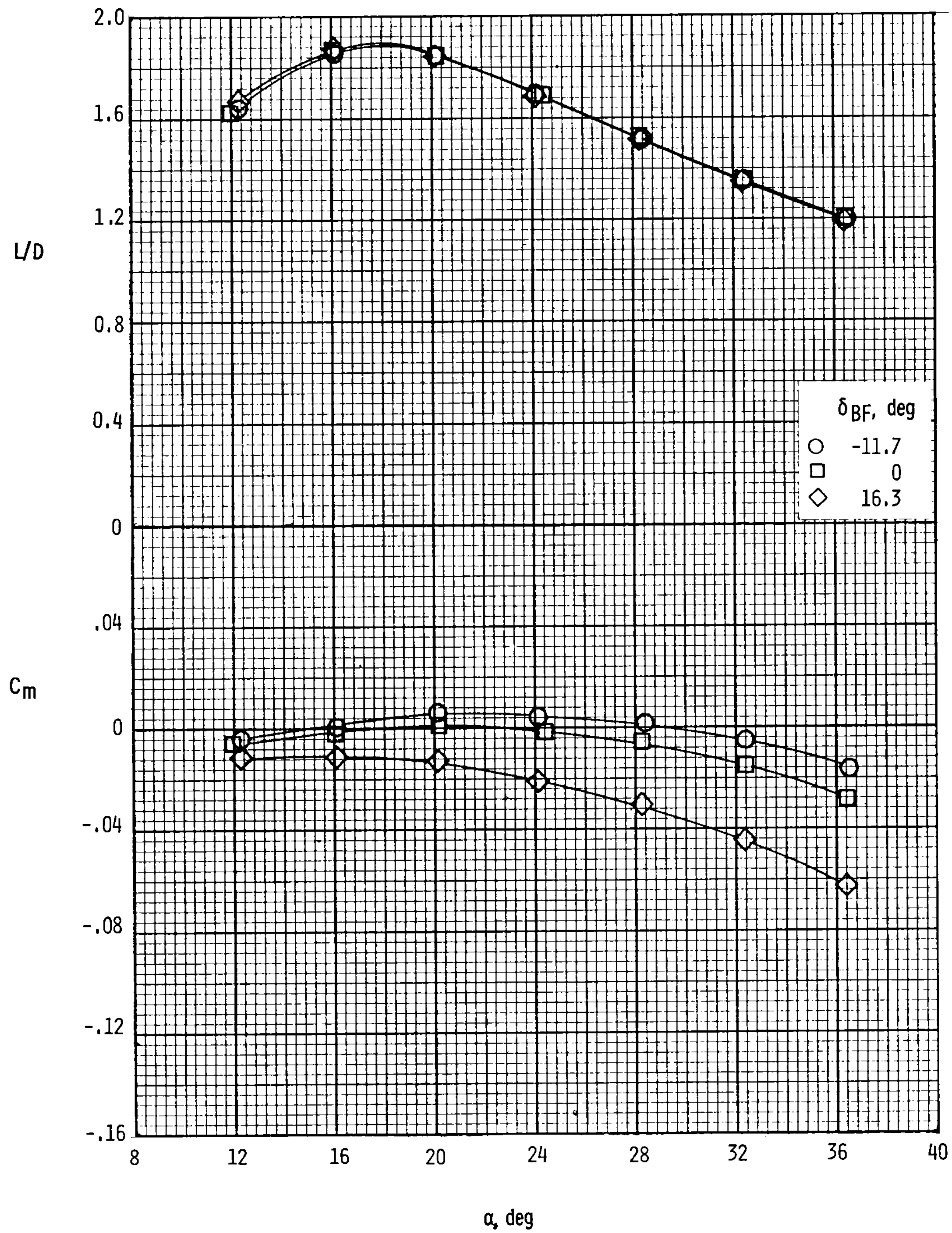

(b) L/D and C_m plotted against α.

Figure 5.- Continued.

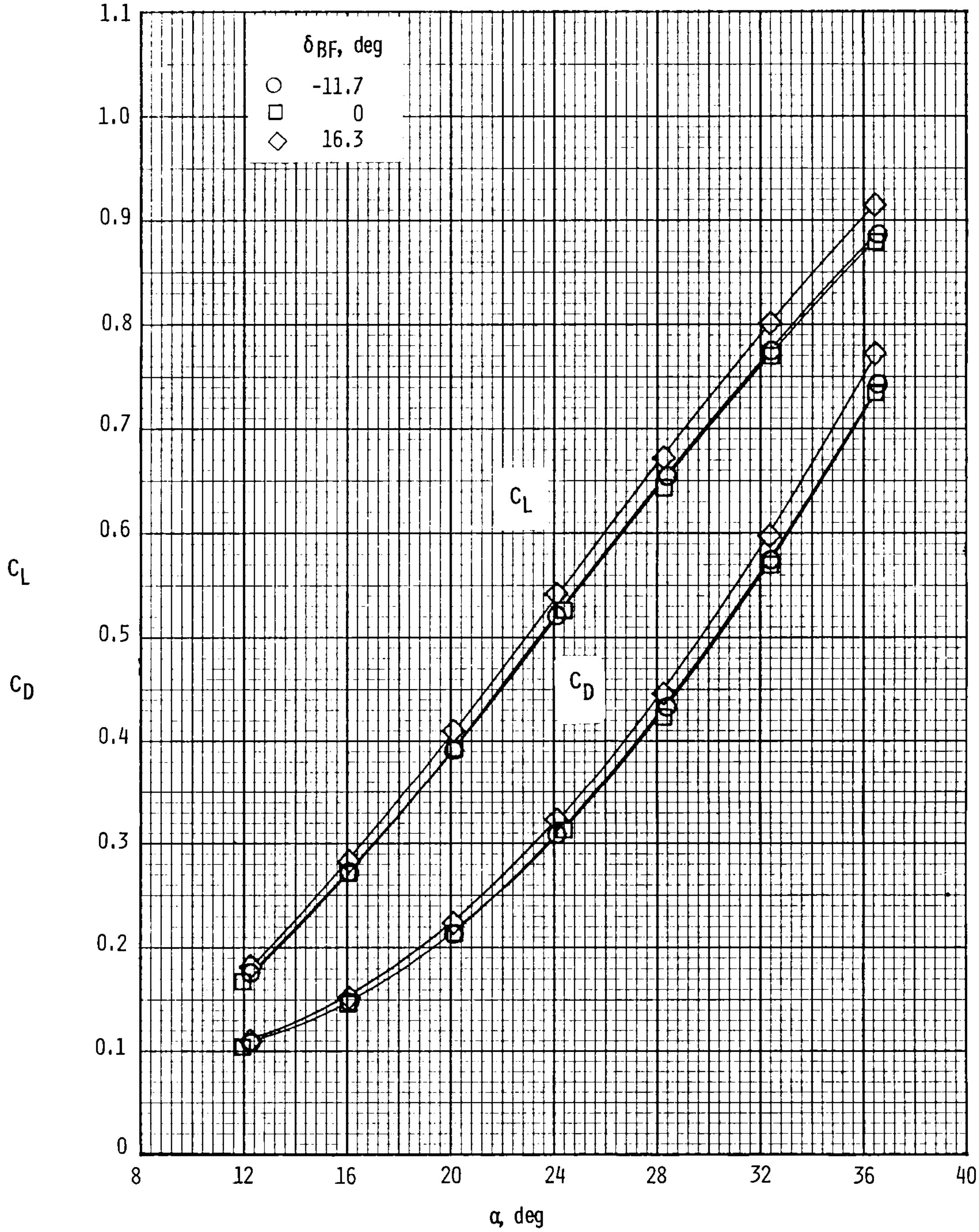

(c) C_L and C_D plotted against α.

Figure 5.- Continued.

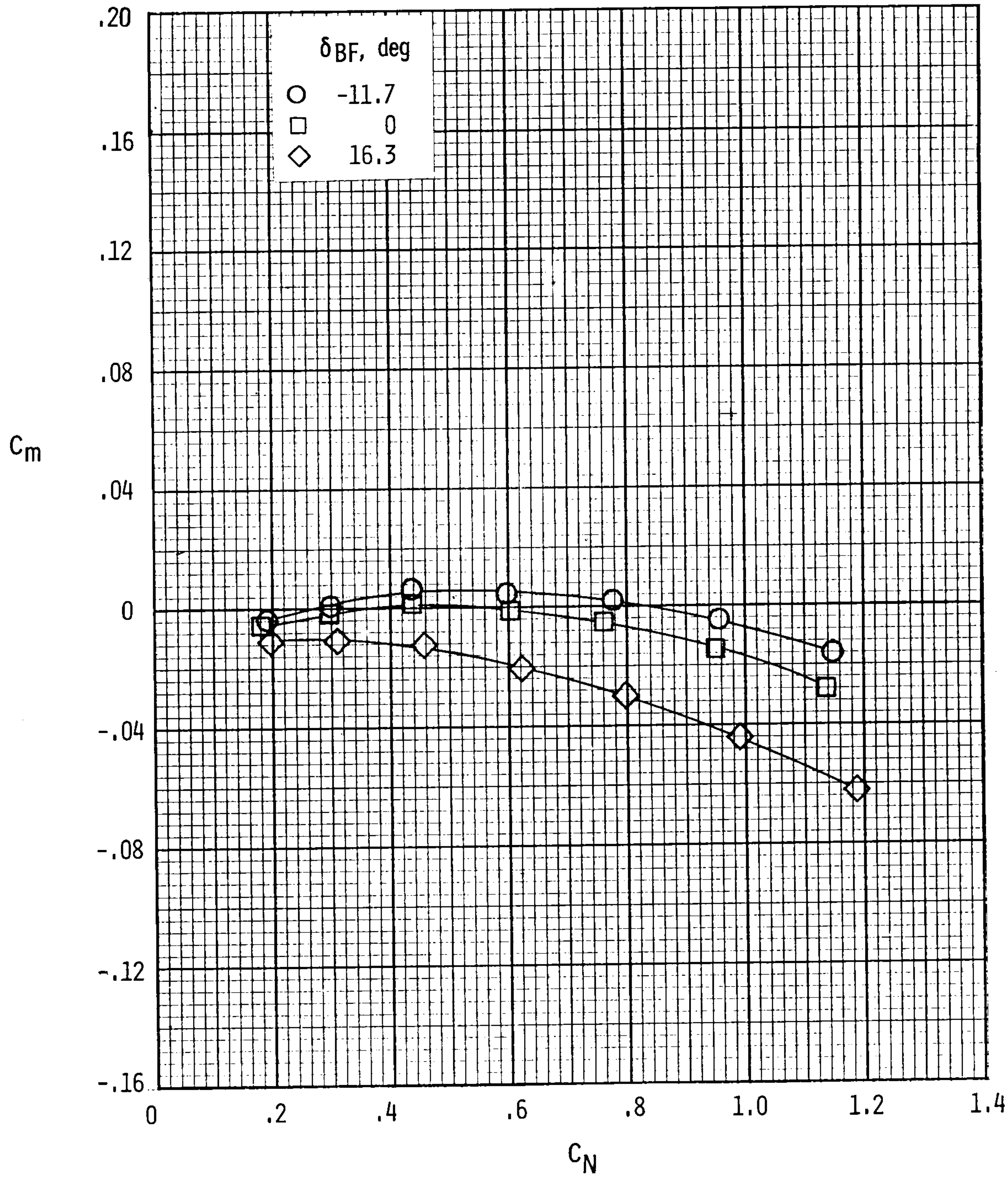

(d) C_m plotted against C_N.

Figure 5.- Concluded.

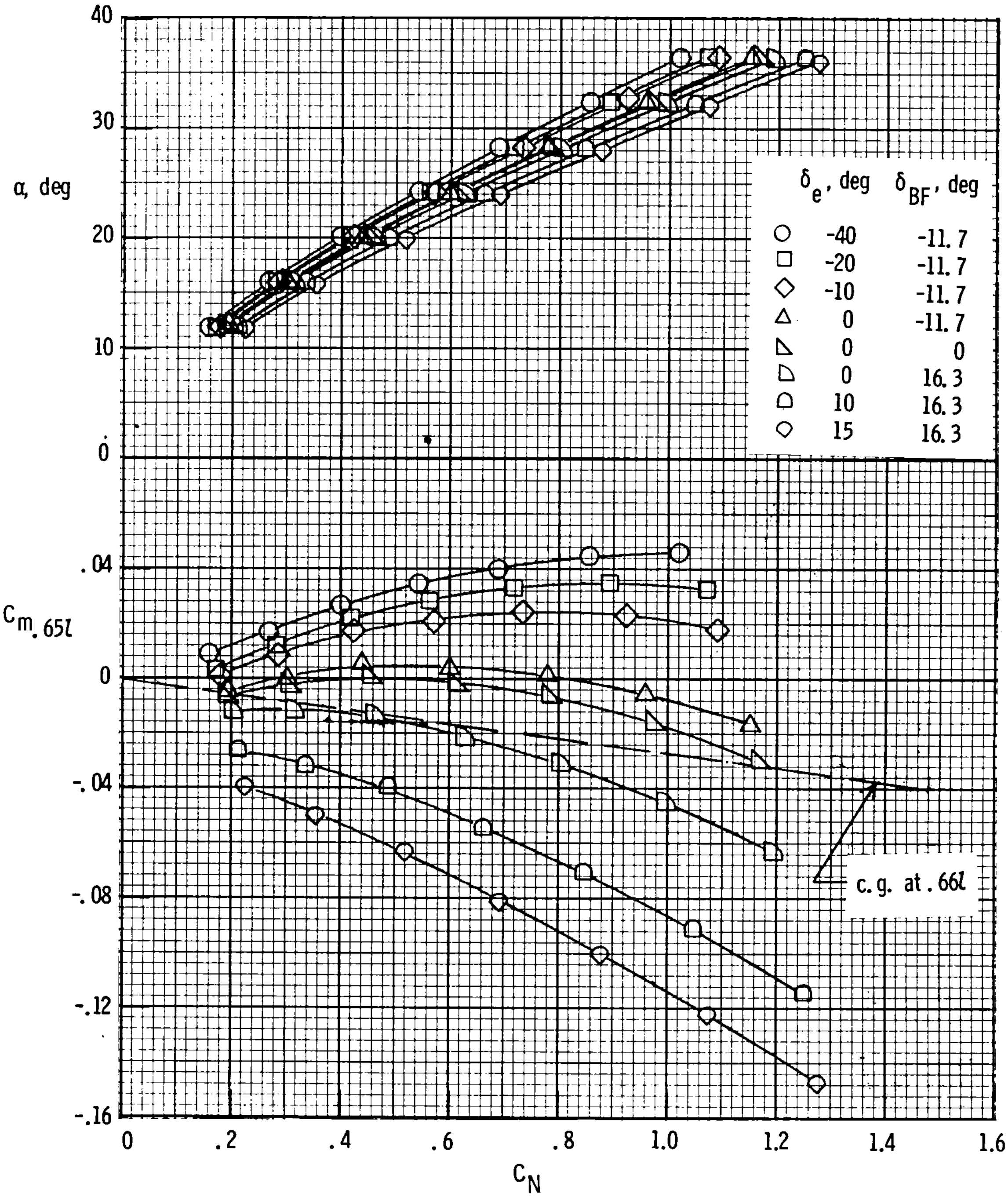

Figure 6.- Summary of elevon and body-flap deflections on longitudinal characteristics. $\delta_{SB} = 55^o$; $R_l = 1.03 \times 10^6$.

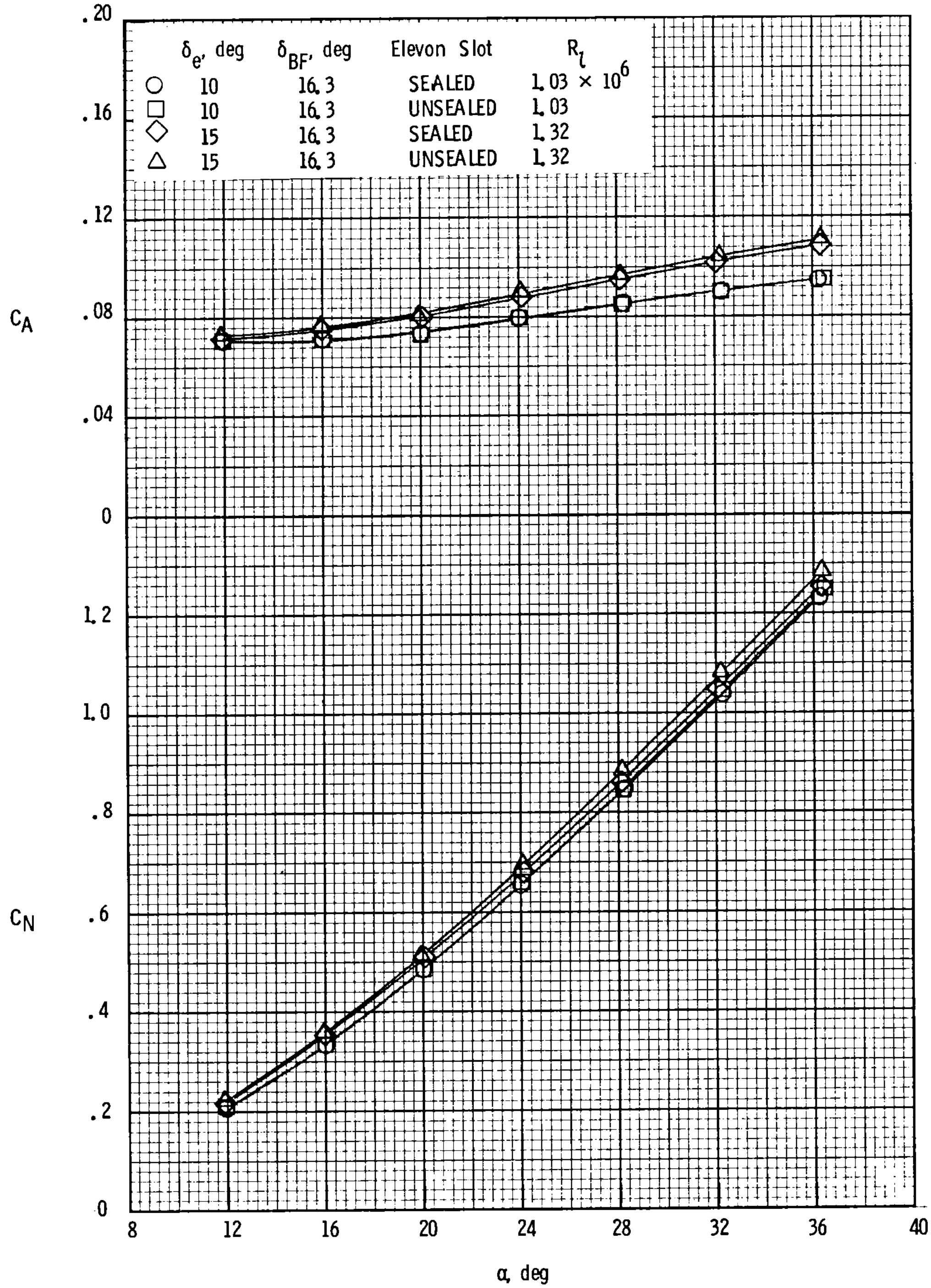

(a) C_A and C_N plotted against α.

Figure 7.- Effects of sealing elevon slots on longitudinal characteristics. $\delta_{SB} = 55^{\circ}$.

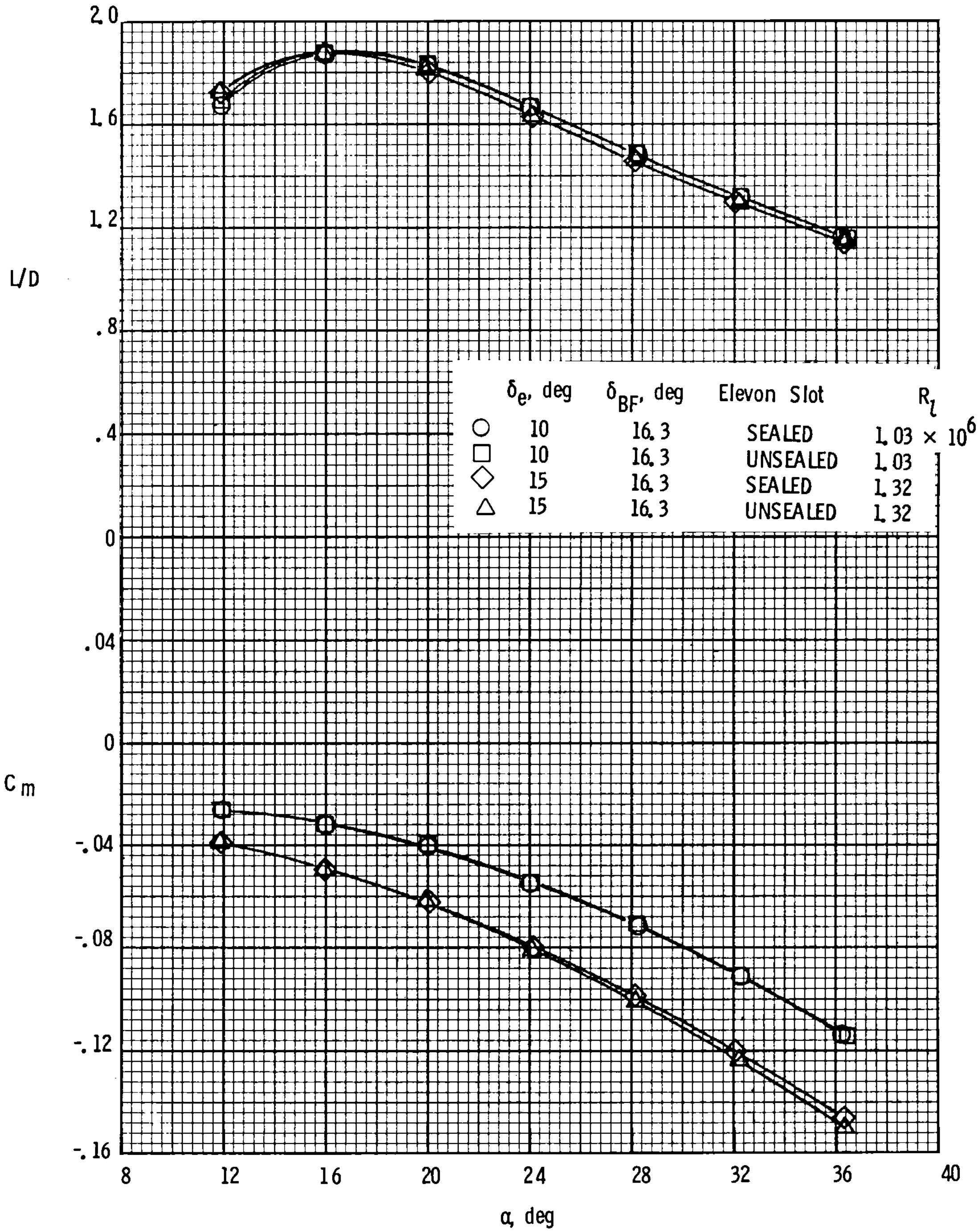

(b) L/D and C_m plotted against α.

Figure 7.- Continued.

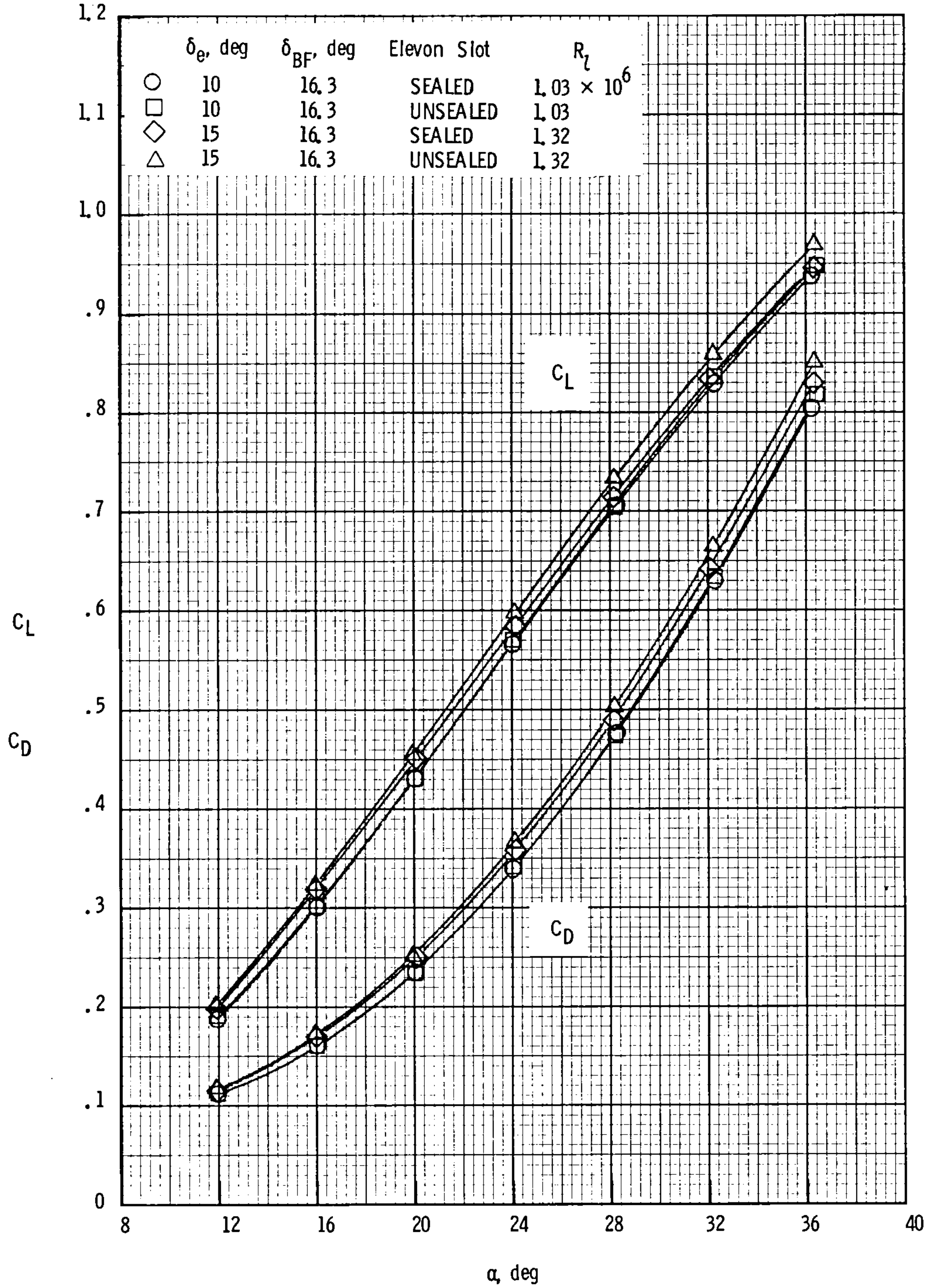

(c) C_L and C_D plotted against α.

Figure 7.- Continued.

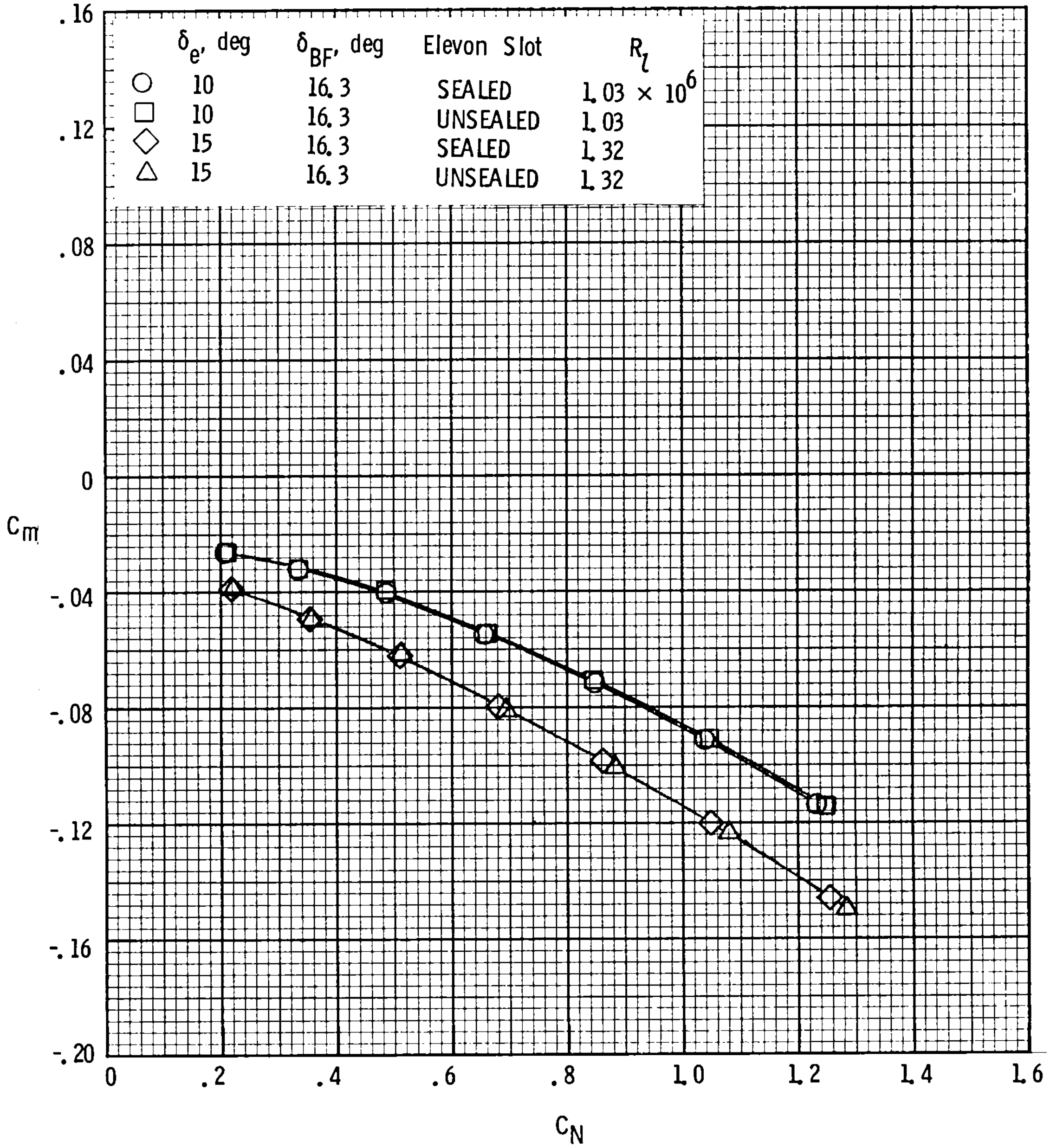

(d) C_m plotted against C_N.

Figure 7.- Concluded.

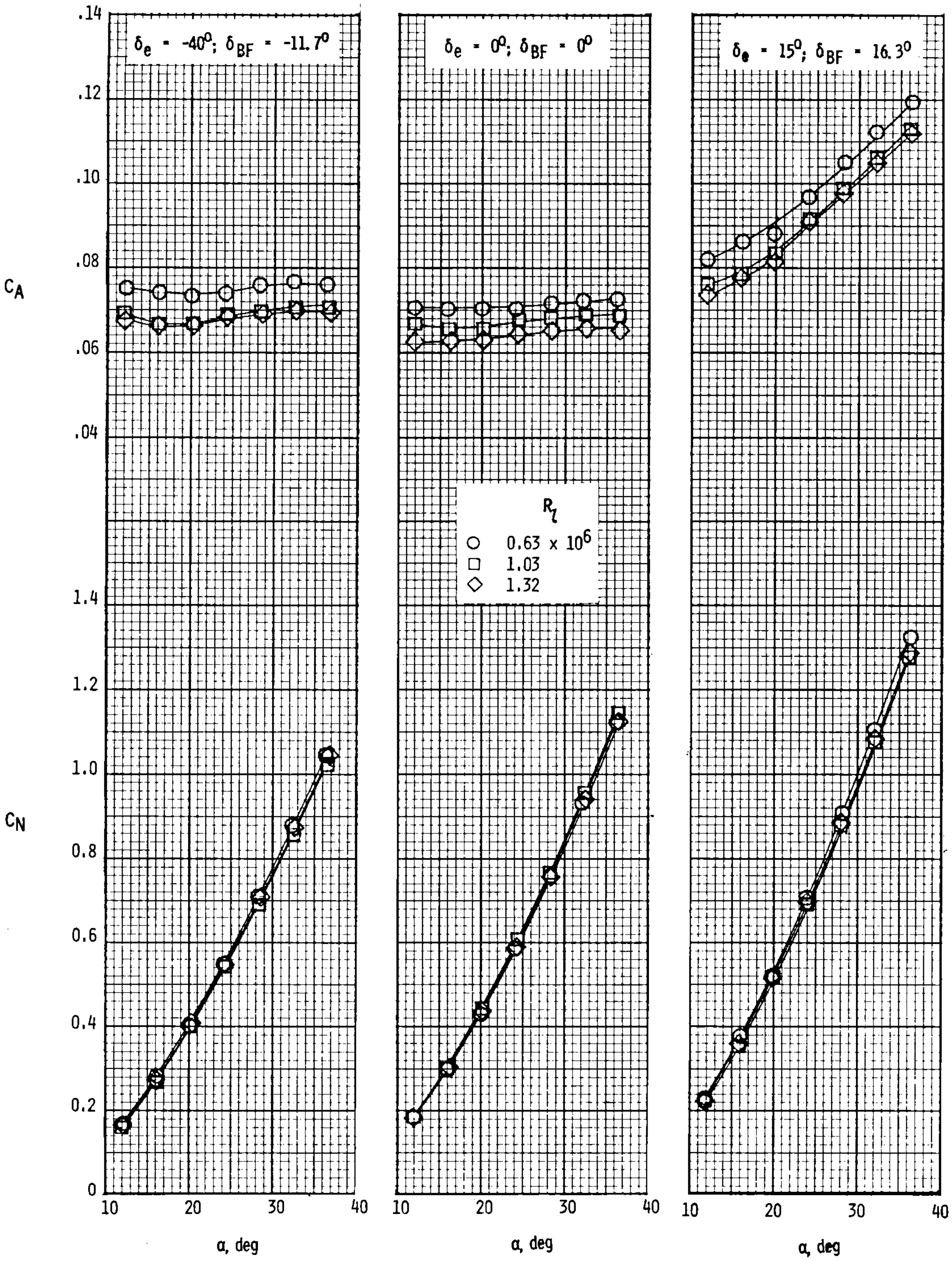

(a) C_A and C_N plotted against α.

Figure 8.- Effects of Reynolds number on longitudinal characteristics. δ_{SB} = 55°.

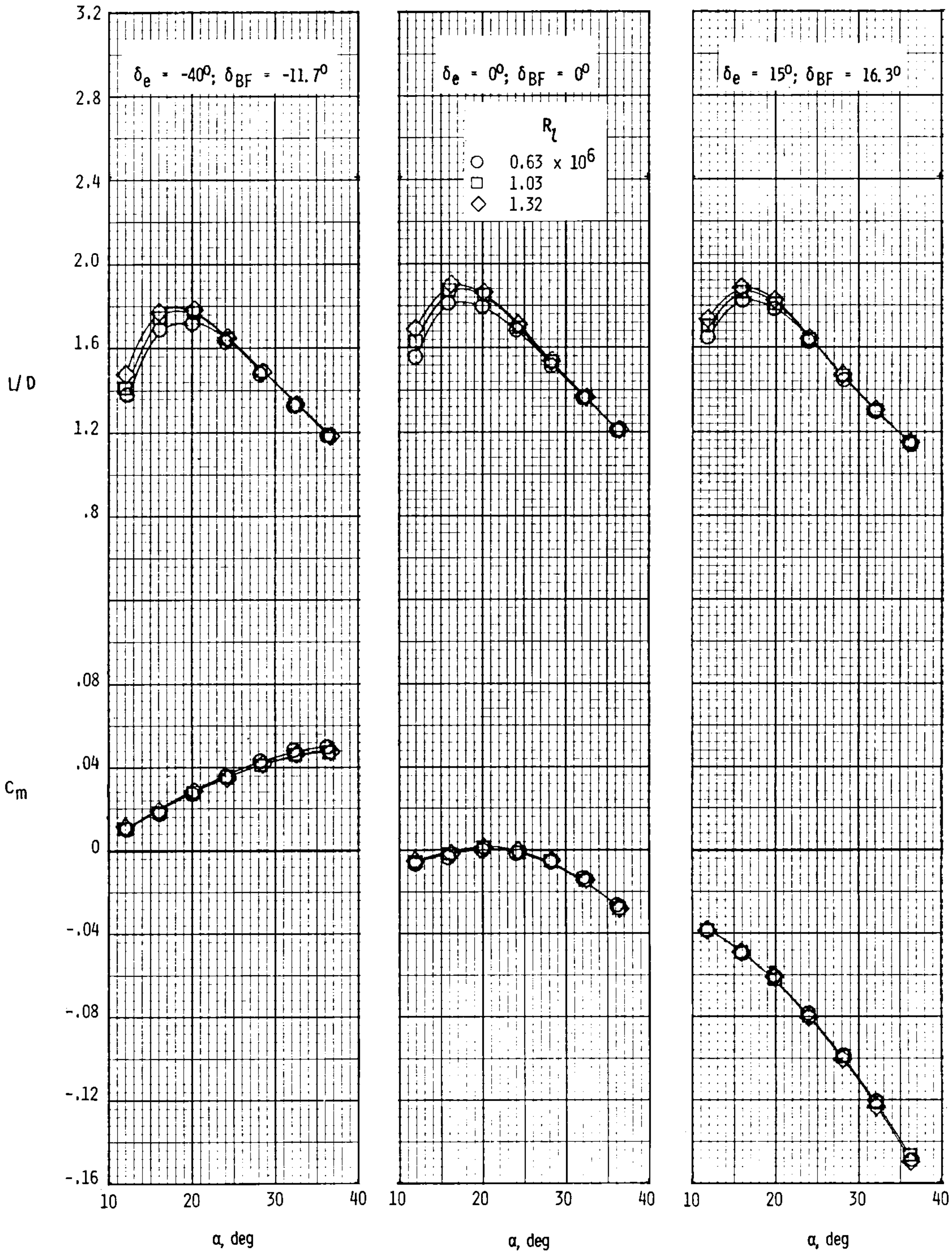

(b) L/D and C_m plotted against α.

Figure 8.- Continued.

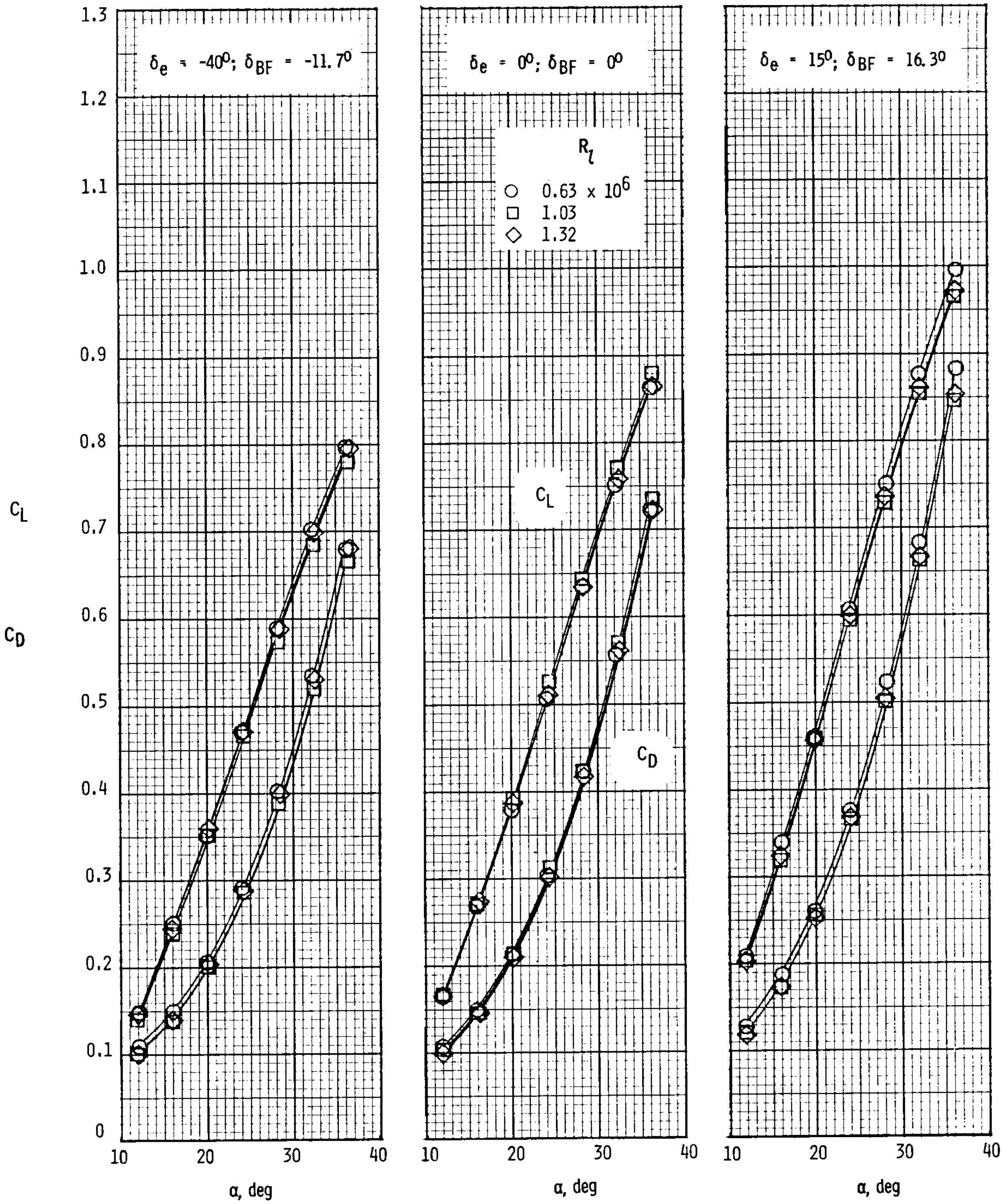

(c) C_L and C_D plotted against α.

Figure 8.- Continued.

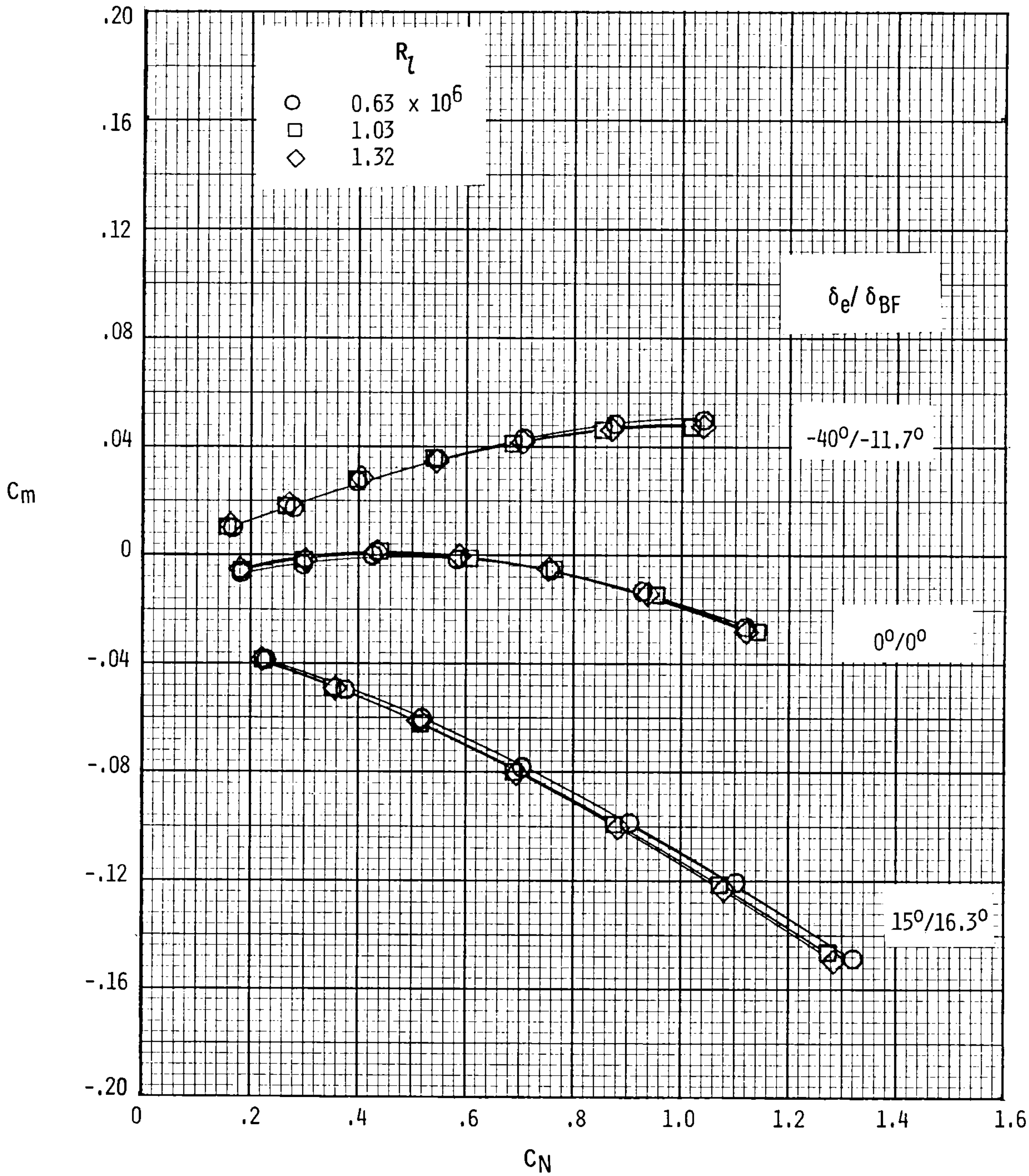

(d) C_m plotted against C_N.

Figure 8.- Concluded.

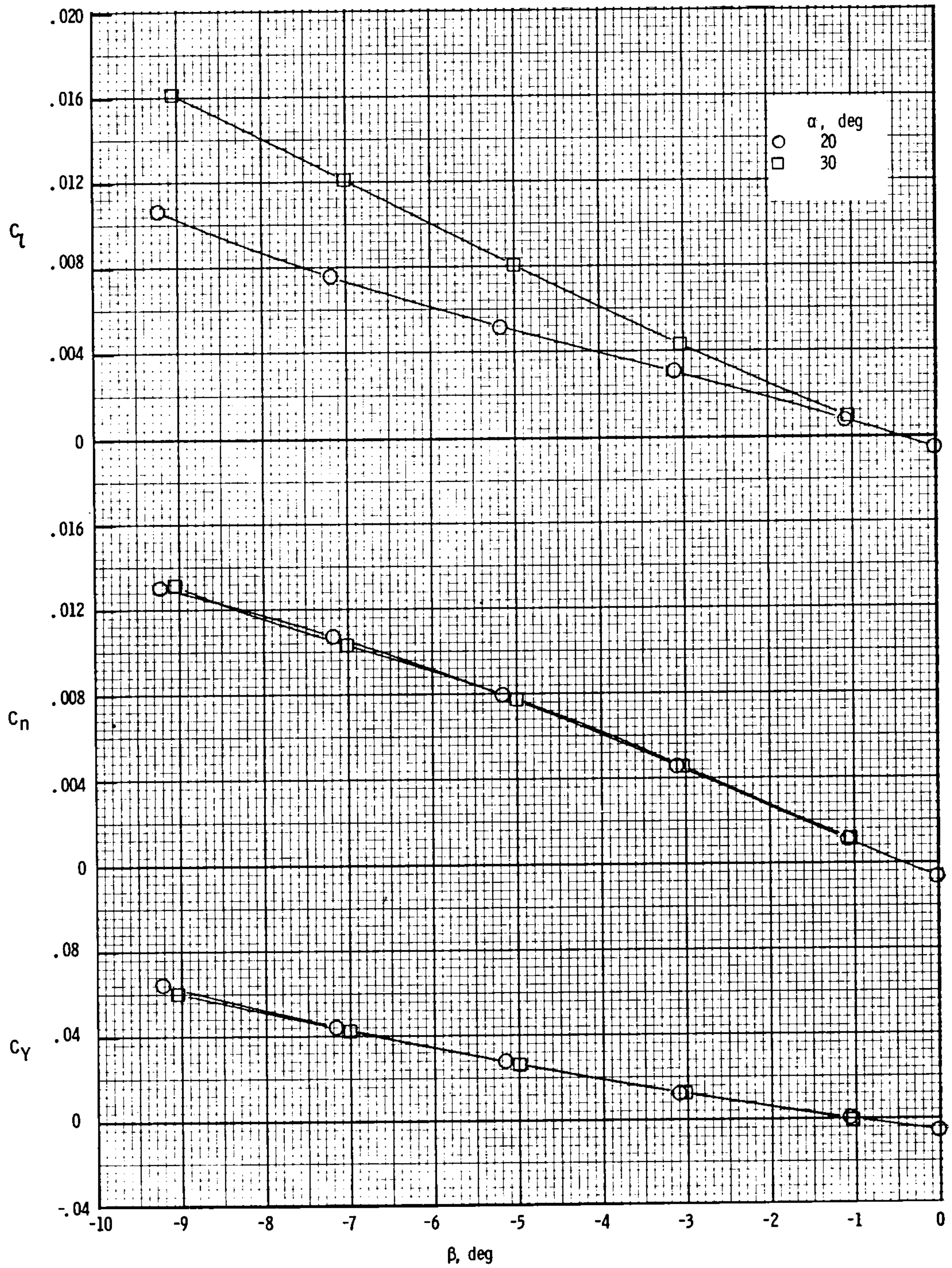

Figure 9.- Variation of lateral-directional coefficients with angle of sideslip. $\delta_e = \delta_{BF} = 0°$, $\delta_{SB} = 55°$, and $R_l = 1.03 \times 10^6$.

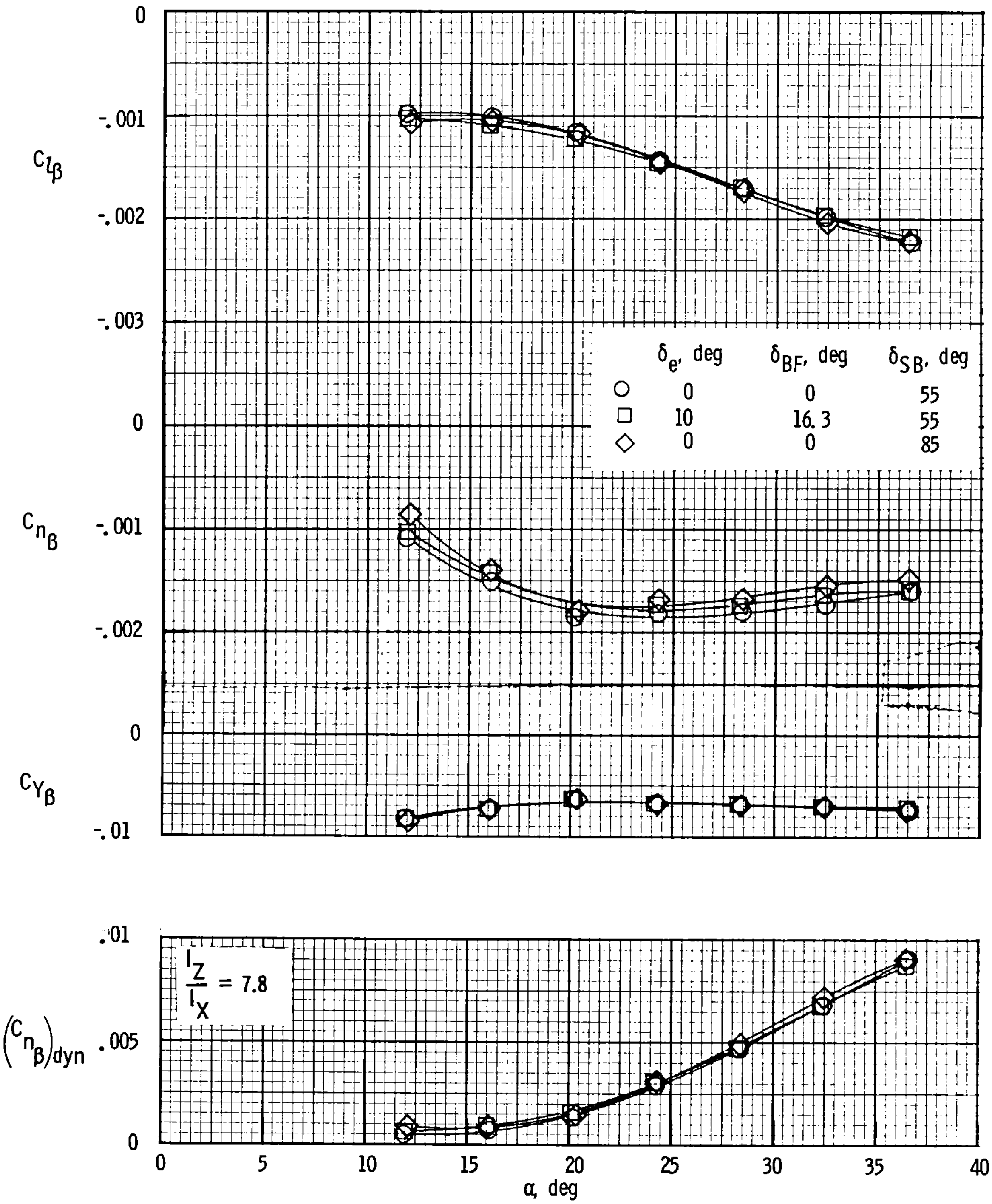

(a) $R_l = 1.03 \times 10^6$.

Figure 10.- Effects of elevon, body-flap, and speed-brake deflections on lateral-directional characteristics.

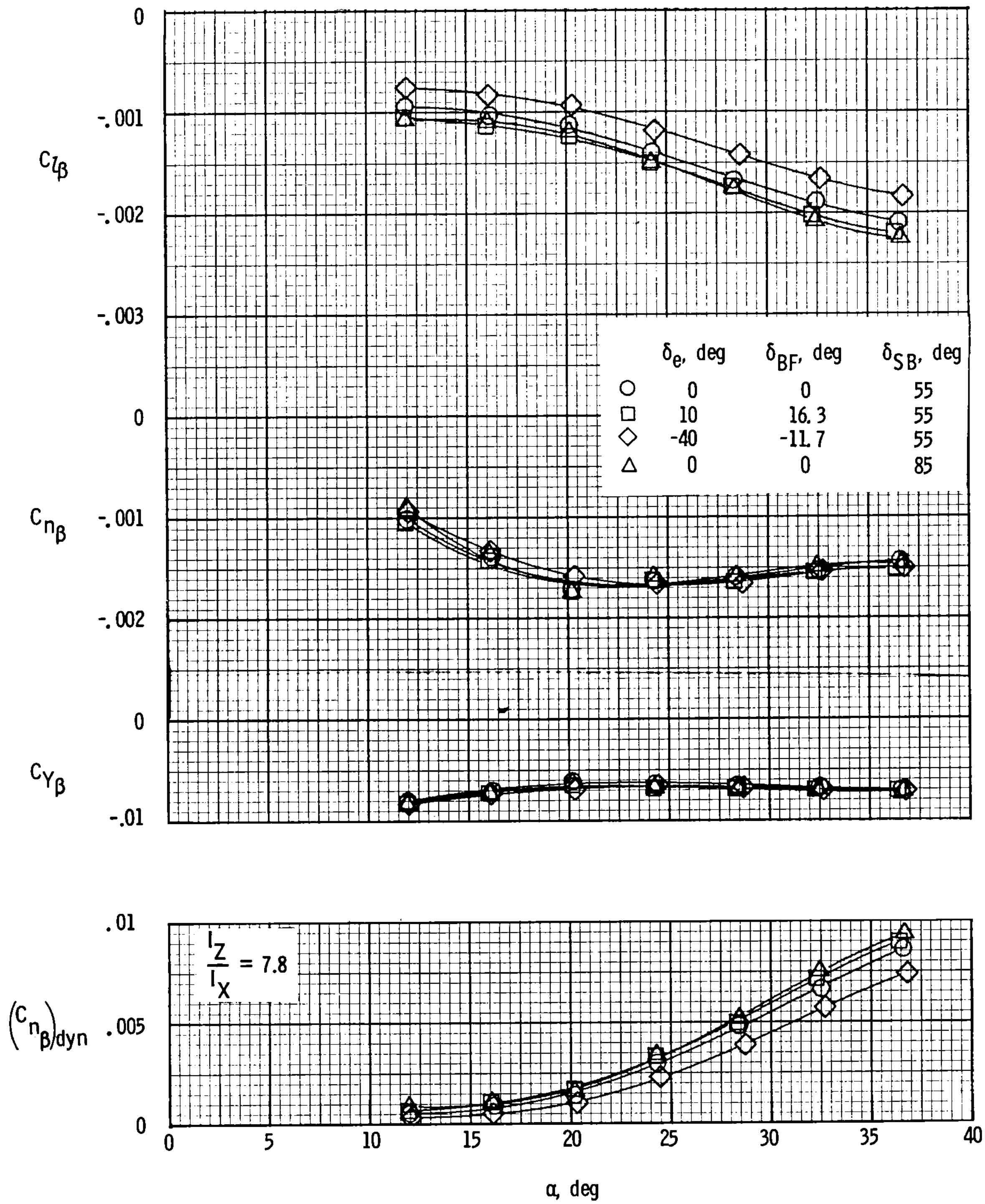

(b) $R_l = 1.33 \times 10^6$.

Figure 10.- Concluded.

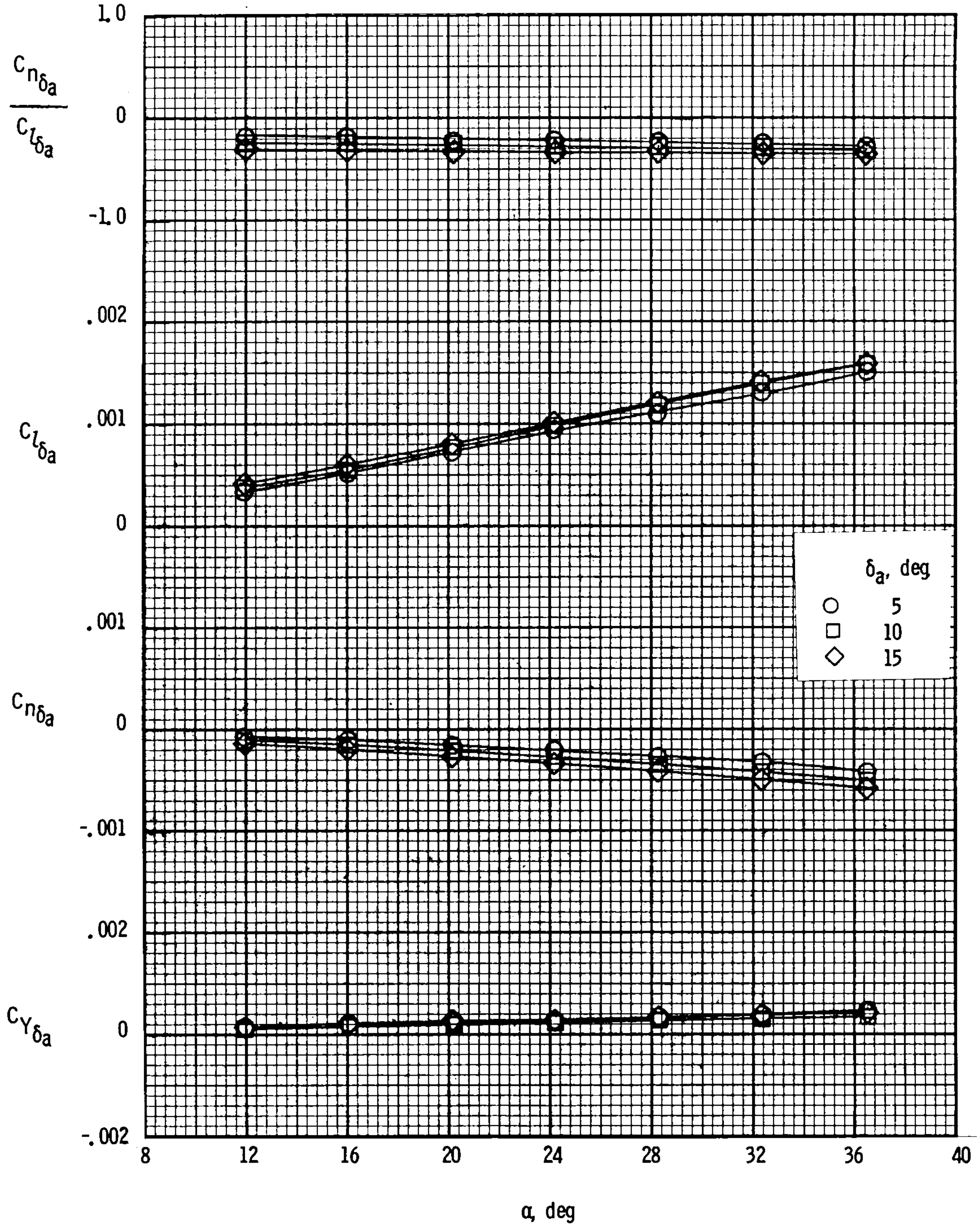

Figure 11.- Effects of aileron deflection on lateral and directional derivatives. $\delta_e = \delta_{BF} = 0^{\circ}$, $\delta_{SB} = 55^{\circ}$, and $R_l = 1.03 \times 10^{6}$.

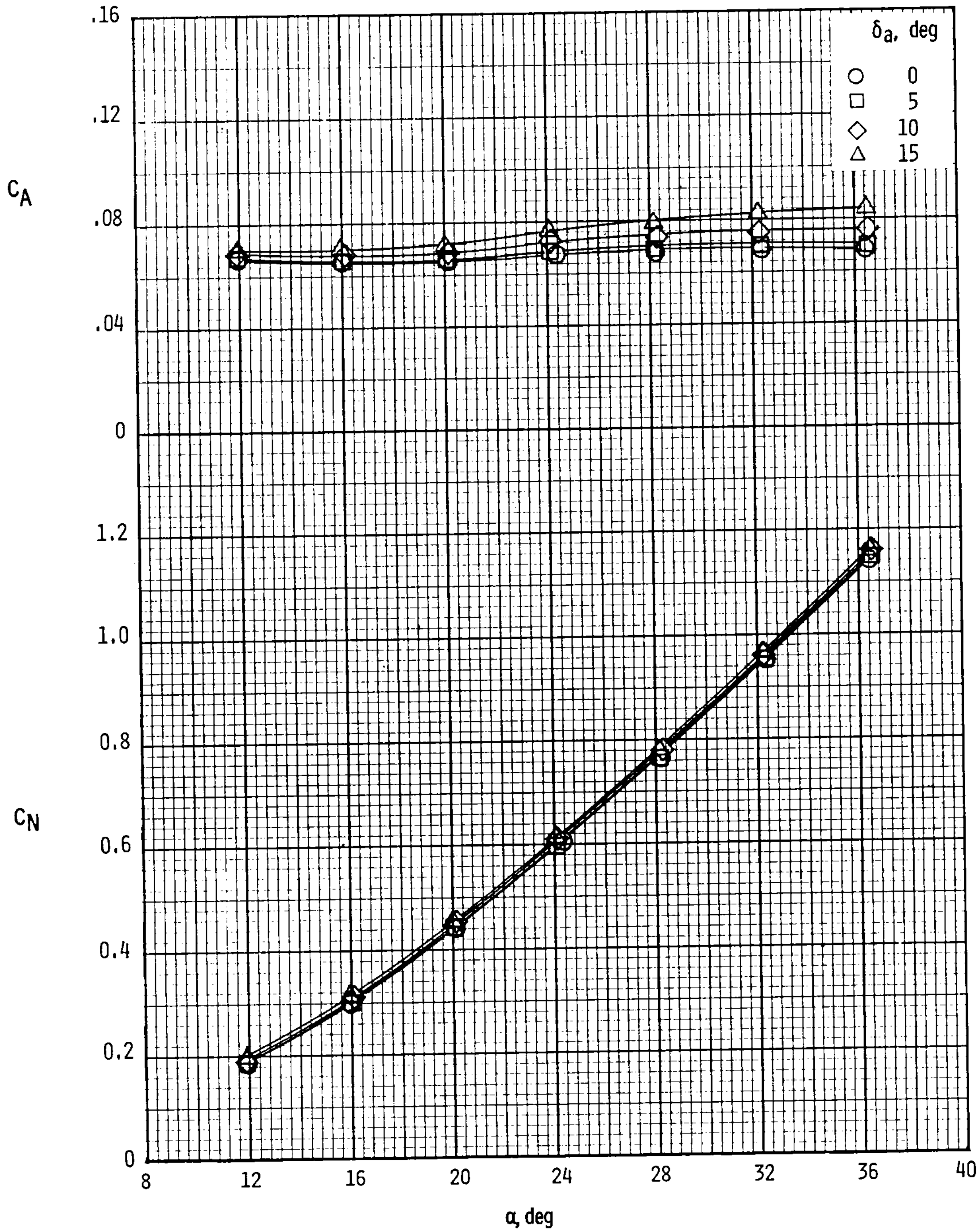

(a) C_A and C_N plotted against α.

Figure 12.- Effects of aileron deflection on longitudinal characteristics. $\delta_e = \delta_{BF} = 0^{\circ}$, $\delta_{SB} = 55^{\circ}$, and $R_l = 1.03 \times 10^6$.

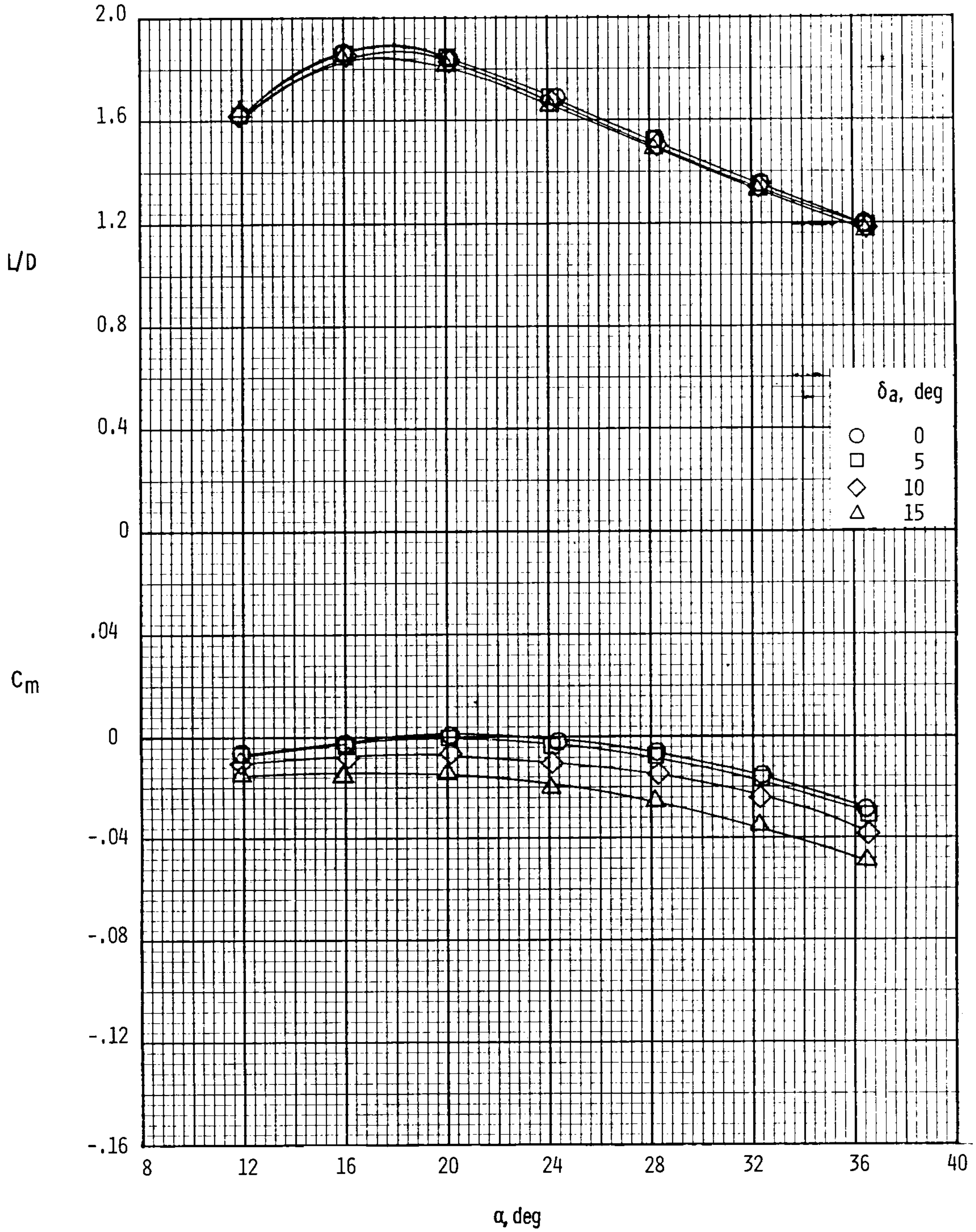

(b) L/D and C_m plotted against α.

Figure 12.- Continued.

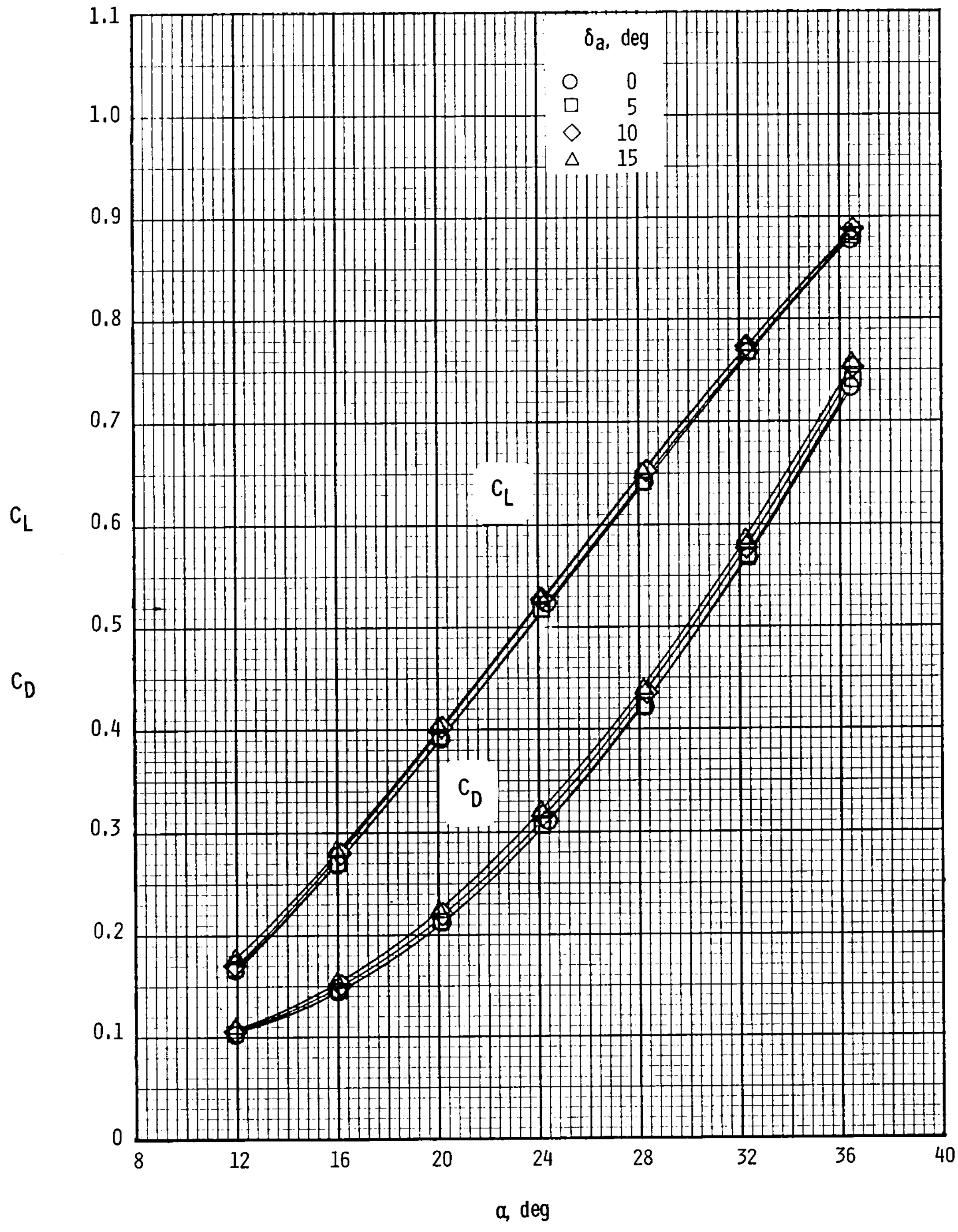

(c) C_L and C_D plotted against α.

Figure 12.- Continued.

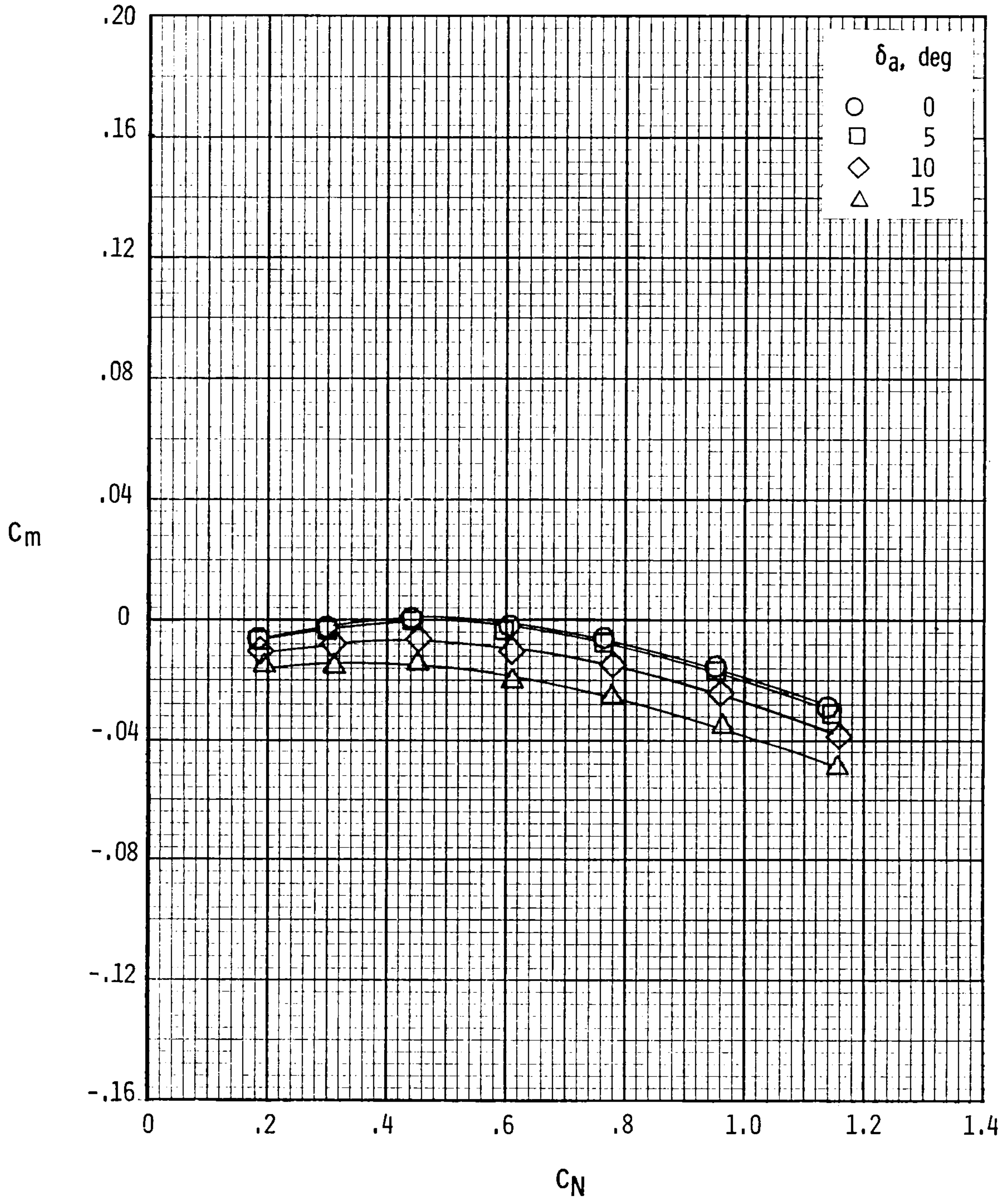

(d) C_m plotted against C_N.

Figure 12.- Concluded.

1. Report No. NASA TM-80086	2. Government Accession No.	3. Recipient's Catalog No.
4. Title and Subtitle AERODYNAMIC CHARACTERISTICS OF THE 140A/B SPACE SHUTTLE ORBITER AT MACH 10.3		5. Report Date May 1979
		6. Performing Organization Code
7. Author(s) Peter T. Bernot		8. Performing Organization Report No. L-12675
9. Performing Organization Name and Address NASA Langley Research Center Hampton, VA 23665		10. Work Unit No. 506-26-13-02
		11. Contract or Grant No.
12. Sponsoring Agency Name and Address National Aeronautics and Space Administration Washington, DC 20546		13. Type of Report and Period Covered Technical Memorandum
		14. Sponsoring Agency Code
15. Supplementary Notes		

16. Abstract

A wind-tunnel investigation has been conducted to determine the static longitudinal and lateral-directional characteristics of the 140A/B space shuttle orbiter configuration. A 0.010-scale model was tested at angles of attack from 12° to 36.5° at Reynolds numbers ranging from 0.62×10^6 to 1.33×10^6 based on fuselage reference length. Stability, control, and performance characteristics were obtained for several deflections of the elevons and body flap. Effects of aileron deflection on roll control and longitudinal stability were also measured. The results indicate that the orbiter is neutrally stable at a 20° angle of attack with control deflections set at 0° and the center of gravity at 65 percent of fuselage length. For a typical entry attitude of 30°, stable trim resulting in a lift-drag ratio of 1.40 is possible. Increasing the Reynolds number yielded higher values of lift-drag ratio, but only for angles of attack up to 24°. The orbiter is directionally unstable with positive dihedral effect. Aileron deflection resulted in adverse yaw to roll control and also caused negative increments in pitching moment over the test angle-of-attack range. This investigation, designated "Rockwell International test OA90," was conducted in the Langley continuous-flow hypersonic tunnel.

17. Key Words (Suggested by Author(s)) Space transportation Hypersonic stability and control	18. Distribution Statement Unclassified - Unlimited Subject Category 16

19. Security Classif. (of this report)	20. Security Classif. (of this page)	21. No. of Pages	22. Price*
Unclassified	Unclassified	44	$4.50

* For sale by the National Technical Information Service, Springfield, Virginia 22161

NASA-Langley, 1979

End of Document